Eur. Phys. J. C 18, 229–252 (2000)
Digital Object Identifier (DOI) 10.1007/s100520000531

THE EUROPEAN PHYSICAL JOURNAL C

Study of B_s^0-$\overline{B_s^0}$ oscillations and B_s^0 lifetimes using hadronic decays of B_s^0 mesons

The DELPHI Collaboration

P. Abreu[22], W. Adam[51], T. Adye[37], P. Adzic[12], I. Ajinenko[43], Z. Albrecht[18], T. Alderweireld[2], G.D. Alekseev[17], R. Alemany[50], T. Allmendinger[18], P.P. Allport[23], S. Almehed[25], U. Amaldi[9], N. Amapane[46], S. Amato[48], E.G. Anassontzis[3], P. Andersson[45], A. Andreazza[9], S. Andringa[22], P. Antilogus[26], W-D. Apel[18], Y. Arnoud[9], B. Åsman[45], J-E. Augustin[26], A. Augustinus[9], P. Baillon[9], P. Bambade[20], F. Barao[22], G. Barbiellini[47], R. Barbier[26], D.Y. Bardin[17], G. Barker[18], A. Baroncelli[39], M. Battaglia[16], M. Baubillier[24], K-H. Becks[53], M. Begalli[6], A. Behrmann[53], P. Beilliere[8], Yu. Belokopytov[9], N.C. Benekos[32], A.C. Benvenuti[5], C. Berat[15], M. Berggren[26], D. Bertini[26], D. Bertrand[2], M. Besancon[40], M. Bigi[46], M.S. Bilenky[17], M-A. Bizouard[20], D. Bloch[10], H.M. Blom[31], M. Bonesini[28], W. Bonivento[28], M. Boonekamp[40], P.S.L. Booth[23], A.W. Borgland[4], G. Borisov[20], C. Bosio[42], O. Botner[49], E. Boudinov[31], B. Bouquet[20], C. Bourdarios[20], T.J.V. Bowcock[23], I. Boyko[17], I. Bozovic[12], M. Bozzo[14], M. Bracko[44], P. Branchini[39], T. Brenke[53], R.A. Brenner[49], P. Bruckman[9], J-M. Brunet[8], L. Bugge[33], T. Buran[33], T. Burgsmueller[53], B. Buschbeck[51], P. Buschmann[53], S. Cabrera[50], M. Caccia[28], M. Calvi[28], T. Camporesi[9], V. Canale[38], F. Carena[9], L. Carroll[23], C. Caso[14], M.V. Castillo Gimenez[50], A. Cattai[9], F.R. Cavallo[5], V. Chabaud[9], Ph. Charpentier[9], L. Chaussard[26], P. Checchia[36], G.A. Chelkov[17], R. Chierici[46], P. Chliapnikov[43], P. Chochula[7], V. Chorowicz[26], J. Chudoba[30], K. Cieslik[19], P. Collins[9], R. Contri[14], E. Cortina[50], G. Cosme[20], F. Cossutti[9], H.B. Crawley[1], D. Crennell[37], S. Crepe[15], G. Crosetti[14], J. Cuevas Maestro[34], S. Czellar[16], M. Davenport[9], W. Da Silva[24], A. Deghorain[2], G. Della Ricca[47], P. Delpierre[27], N. Demaria[9], A. De Angelis[9], W. De Boer[18], C. De Clercq[2], B. De Lotto[47], A. De Min[36], L. De Paula[48], H. Dijkstra[9], L. Di Ciaccio[38,9], J. Dolbeau[8], K. Doroba[52], M. Dracos[10], J. Drees[53], M. Dris[32], A. Duperrin[26], J-D. Durand[9], G. Eigen[4], T. Ekelof[49], G. Ekspong[45], M. Ellert[49], M. Elsing[9], J-P. Engel[10], M. Espirito Santo[22], G. Fanourakis[12], D. Fassouliotis[12], J. Fayot[24], M. Feindt[18], A. Fenyuk[43], P. Ferrari[28], A. Ferrer[50], E. Ferrer-Ribas[20], F. Ferro[14], S. Fichet[24], A. Firestone[1], U. Flagmeyer[53], H. Foeth[9], E. Fokitis[32], F. Fontanelli[14], B. Franek[37], A.G. Frodesen[4], R. Fruhwirth[51], F. Fulda-Quenzer[20], J. Fuster[50], A. Galloni[23], D. Gamba[46], S. Gamblin[20], M. Gandelman[48], C. Garcia[50], C. Gaspar[9], M. Gaspar[48], U. Gasparini[36], Ph. Gavillet[9], E.N. Gazis[32], D. Gele[10], N. Ghodbane[26], I. Gil[50], F. Glege[53], R. Gokieli[9,52], B. Golob[44], G. Gomez-Ceballos[41], P. Goncalves[22], I. Gonzalez Caballero[41], G. Gopal[37], L. Gorn[1,54], Yu. Gouz[43], V. Gracco[14], J. Grahl[1], E. Graziani[39], H-J. Grimm[18], P. Gris[40], G. Grosdidier[20], K. Grzelak[52], M. Gunther[49], J. Guy[37], F. Hahn[9], S. Hahn[53], S. Haider[9], A. Hallgren[49], K. Hamacher[53], J. Hansen[33], F.J. Harris[35], V. Hedberg[25], S. Heising[18], J.J. Hernandez[50], P. Herquet[2], H. Herr[9], T.L. Hessing[35], J.-M. Heuser[53], E. Higon[50], S-O. Holmgren[45], P.J. Holt[35], S. Hoorelbeke[2], M. Houlden[23], J. Hrubec[51], K. Huet[2], G.J. Hughes[23], K. Hultqvist[45], J.N. Jackson[23], R. Jacobsson[9], P. Jalocha[19], R. Janik[7], Ch. Jarlskog[25], G. Jarlskog[25], P. Jarry[40], B. Jean-Marie[20], D. Jeans[35], E.K. Johansson[45], P. Jonsson[26], C. Joram[9], P. Juillot[10], F. Kapusta[24], K. Karafasoulis[12], S. Katsanevas[26], E.C. Katsoufis[32], R. Keranen[18], G. Kernel[44], B.P. Kersevan[44], B.A. Khomenko[17], N.N. Khovanski[17], A. Kiiskinen[16], B. King[23], A. Kinvig[23], N.J. Kjaer[31], O. Klapp[53], H. Klein[9], P. Kluit[31], P. Kokkinias[12], M. Koratzinos[9], V. Kostioukhine[43], C. Kourkoumelis[3], O. Kouznetsov[40], M. Krammer[51], E. Kriznic[44], Z. Krumstein[17], P. Kubinec[7], J. Kurowska[52], K. Kurvinen[16], J.W. Lamsa[1], D.W. Lane[1], P. Langefeld[53], V. Lapin[43], J-P. Laugier[40], R. Lauhakangas[16], G. Leder[51], F. Ledroit[15], V. Lefebure[2], L. Leinonen[45], A. Leisos[12], R. Leitner[30], J. Lemonne[2], G. Lenzen[53], V. Lepeltier[20], T. Lesiak[19], M. Lethuillier[40], J. Libby[35], D. Liko[9], A. Lipniacka[45], I. Lippi[36], B. Loerstad[25], J.G. Loken[35], J.H. Lopes[48], J.M. Lopez[41], R. Lopez-Fernandez[15], D. Loukas[12], P. Lutz[40], L. Lyons[35], J. MacNaughton[51], J.R. Mahon[6], A. Maio[22], A. Malek[53], T.G.M. Malmgren[45], S. Maltezos[32], V. Malychev[17], F. Mandl[51], J. Marco[41], R. Marco[41], B. Marechal[48], M. Margoni[36], J-C. Marin[9], C. Mariotti[9], A. Markou[12], C. Martinez-Rivero[20], F. Martinez-Vidal[50], S. Marti i Garcia[9], J. Masik[13], N. Mastroyiannopoulos[12], F. Matorras[41], C. Matteuzzi[28], G. Matthiae[38], F. Mazzucato[36], M. Mazzucato[36], M. Mc Cubbin[23], R. Mc Kay[1], R. Mc Nulty[23], G. Mc Pherson[23], C. Meroni[28], W.T. Meyer[1], A. Miagkov[43], E. Migliore[9], L. Mirabito[26], W.A. Mitaroff[51], U. Mjoernmark[25], T. Moa[45], M. Moch[18], R. Moeller[29], K. Moenig[9,11], M.R. Monge[14], X. Moreau[24], P. Morettini[14], G. Morton[35], U. Mueller[53], K. Muenich[53], M. Mulders[31], C. Mulet-Marquis[15], R. Muresan[25], W.J. Murray[37], B. Muryn[15,19], G. Myatt[35], T. Myklebust[33], F. Naraghi[15], M. Nassiakou[12], F.L. Navarria[5], S. Navas[50], K. Nawrocki[52], P. Negri[28], N. Neufeld[9], R. Nicolaidou[40], B.S. Nielsen[29], P. Niezurawski[52], M. Nikolenko[10,17], V. Nomokonov[16], A. Nygren[25], V. Obraztsov[43], A.G. Olshevski[17], A. Onofre[22], R. Orava[16], G. Orazi[10], K. Osterberg[16],

A. Ouraou[40], M. Paganoni[28], S. Paiano[5], R. Pain[24], R. Paiva[22], J. Palacios[35], H. Palka[19], Th.D. Papadopoulou[32,9], K. Papageorgiou[12], L. Pape[9], C. Parkes[9], F. Parodi[14], U. Parzefall[23], A. Passeri[39], O. Passon[53], T. Pavel[25], M. Pegoraro[36], L. Peralta[22], M. Pernicka[51], A. Perrotta[5], C. Petridou[47], A. Petrolini[14], H.T. Phillips[37], F. Pierre[40], M. Pimenta[22], E. Piotto[28], T. Podobnik[44], M.E. Pol[6], G. Polok[19], P. Poropat[47], V. Pozdniakov[17], P. Privitera[38], N. Pukhaeva[17], A. Pullia[28], D. Radojicic[35], S. Ragazzi[28], H. Rahmani[32], J. Rames[13], P.N. Ratoff[21], A.L. Read[33], P. Rebecchi[9], N.G. Redaelli[28], M. Regler[51], D. Reid[31], R. Reinhardt[53], P.B. Renton[35], L.K. Resvanis[3], F. Richard[20], J. Ridky[13], G. Rinaudo[46], O. Rohne[33], A. Romero[46], P. Ronchese[36], E.I. Rosenberg[1], P. Rosinsky[7], P. Roudeau[20], T. Rovelli[5], Ch. Royon[40], V. Ruhlmann-Kleider[40], A. Ruiz[41], H. Saarikko[16], Y. Sacquin[40], A. Sadovsky[17], G. Sajot[15], J. Salt[50], D. Sampsonidis[12], M. Sannino[14], H. Schneider[18], Ph. Schwemling[24], B. Schwering[53], U. Schwickerath[18], F. Scuri[47], P. Seager[21], Y. Sedykh[17], A.M. Segar[35], R. Sekulin[37], R.C. Shellard[6], M. Siebel[53], L. Simard[40], F. Simonetto[36], A.N. Sisakian[17], G. Smadja[26], N. Smirnov[43], O. Smirnova[25], G.R. Smith[37], A. Sokolov[43], A. Sopczak[18], R. Sosnowski[52], T. Spassov[22], E. Spiriti[39], P. Sponholz[53], S. Squarcia[14], C. Stanescu[39], S. Stanic[44], K. Stevenson[35], A. Stocchi[20], J. Strauss[51], R. Strub[10], B. Stugu[4], M. Szczekowski[52], M. Szeptycka[52], T. Tabarelli[28], A. Taffard[23], F. Tegenfeldt[49], F. Terranova[28], J. Thomas[35], J. Timmermans[31], N. Tinti[5], L.G. Tkatchev[17], M. Tobin[23], S. Todorova[10], A. Tomaradze[2], B. Tome[22], A. Tonazzo[9], L. Tortora[39], P. Tortosa[50], G. Transtromer[25], D. Treille[9], G. Tristram[8], M. Trochimczuk[52], C. Troncon[28], A. Tsirou[9], M-L. Turluer[40], I.A. Tyapkin[17], S. Tzamarias[12], O. Ullaland[9], V. Uvarov[43], G. Valenti[5], E. Vallazza[47], C. Vander Velde[2], G.W. Van Apeldoorn[31], P. Van Dam[31], W. Van Den Boeck[2], W.K. Van Doninck[2], J. Van Eldik[31], A. Van Lysebetten[2], N. Van Remortel[2], I. Van Vulpen[31], G. Vegni[28], L. Ventura[36], W. Venus[37,9], F. Verbeure[2], M. Verlato[36], L.S. Vertogradov[17], V. Verzi[38], D. Vilanova[40], L. Vitale[47], E. Vlasov[43], A.S. Vodopyanov[17], C. Vollmer[18], G. Voulgaris[3], V. Vrba[13], H. Wahlen[53], C. Walck[45], A.J. Washbrook[23], C. Weiser[18], D. Wicke[53], J.H. Wickens[2], G.R. Wilkinson[9], M. Winter[10], M. Witek[19], G. Wolf[9], J. Yi[1], O. Yushchenko[43], A. Zalewska[19], P. Zalewski[52], D. Zavrtanik[44], E. Zevgolatakos[12], N.I. Zimin[17,25], A. Zintchenko[17], G.C. Zucchelli[45], G. Zumerle[36]

[1] Department of Physics and Astronomy, Iowa State University, Ames IA 50011-3160, USA
[2] Physics Department, Univ. Instelling Antwerpen, Universiteitsplein 1, 2610 Wilrijk, Belgium
and IIHE, ULB-VUB, Pleinlaan 2, 1050 Brussels, Belgium
and Faculté des Sciences, Univ. de l'Etat Mons, Av. Maistriau 19, 7000 Mons, Belgium
[3] Physics Laboratory, University of Athens, Solonos Str. 104, 10680 Athens, Greece
[4] Department of Physics, University of Bergen, Allégaten 55, 5007 Bergen, Norway
[5] Dipartimento di Fisica, Università di Bologna and INFN, Via Irnerio 46, 40126 Bologna, Italy
[6] Centro Brasileiro de Pesquisas Físicas, rua Xavier Sigaud 150, 22290 Rio de Janeiro, Brazil
and Depto. de Física, Pont. Univ. Católica, C.P. 38071, 22453 Rio de Janeiro, Brazil
and Inst. de Física, Univ. Estadual do Rio de Janeiro, rua São Francisco Xavier 524, Rio de Janeiro, Brazil
[7] Comenius University, Faculty of Mathematics and Physics, Mlynska Dolina, 84215 Bratislava, Slovakia
[8] Collège de France, Lab. de Physique Corpusculaire, IN2P3-CNRS, 75231 Paris Cedex 05, France
[9] CERN, 1211 Geneva 23, Switzerland
[10] Institut de Recherches Subatomiques, IN2P3 - CNRS/ULP - BP20, 67037 Strasbourg Cedex, France
[11] DESY-Zeuthen, Platanenallee 6, 15735 Zeuthen, Germany
[12] Institute of Nuclear Physics, N.C.S.R. Demokritos, P.O. Box 60228, 15310 Athens, Greece
[13] FZU, Inst. of Phys. of the C.A.S. High Energy Physics Division, Na Slovance 2, 180 40, Praha 8, Czech Republic
[14] Dipartimento di Fisica, Università di Genova and INFN, Via Dodecaneso 33, 16146 Genova, Italy
[15] Institut des Sciences Nucléaires, IN2P3-CNRS, Université de Grenoble 1, 38026 Grenoble Cedex, France
[16] Helsinki Institute of Physics, HIP, P.O. Box 9, 00014 Helsinki, Finland
[17] Joint Institute for Nuclear Research, Dubna, Head Post Office, P.O. Box 79, 101 000 Moscow, Russian Federation
[18] Institut für Experimentelle Kernphysik, Universität Karlsruhe, Postfach 6980, 76128 Karlsruhe, Germany
[19] Institute of Nuclear Physics and University of Mining and Metalurgy, Ul. Kawiory 26a, 30055 Krakow, Poland
[20] Université de Paris-Sud, Lab. de l'Accélérateur Linéaire, IN2P3-CNRS, Bât. 200, 91405 Orsay Cedex, France
[21] School of Physics and Chemistry, University of Lancaster, Lancaster LA1 4YB, UK
[22] LIP, IST, FCUL - Av. Elias Garcia, 14-1^o, 1000 Lisboa Codex, Portugal
[23] Department of Physics, University of Liverpool, P.O. Box 147, Liverpool L69 3BX, UK
[24] LPNHE, IN2P3-CNRS, Univ. Paris VI et VII, Tour 33 (RdC), 4 place Jussieu, 75252 Paris Cedex 05, France
[25] Department of Physics, University of Lund, Sölvegatan 14, 223 63 Lund, Sweden
[26] Université Claude Bernard de Lyon, IPNL, IN2P3-CNRS, 69622 Villeurbanne Cedex, France
[27] Univ. d'Aix - Marseille II - CPP, IN2P3-CNRS, 13288 Marseille Cedex 09, France
[28] Dipartimento di Fisica, Università di Milano and INFN, Via Celoria 16, 20133 Milan, Italy
[29] Niels Bohr Institute, Blegdamsvej 17, 2100 Copenhagen Ø, Denmark
[30] NC, Nuclear Centre of MFF, Charles University, Areal MFF, V Holesovickach 2, 180 00, Praha 8, Czech Republic
[31] NIKHEF, Postbus 41882, 1009 DB Amsterdam, The Netherlands
[32] National Technical University, Physics Department, Zografou Campus, 15773 Athens, Greece
[33] Physics Department, University of Oslo, Blindern, 1000 Oslo 3, Norway
[34] Dpto. Fisica, Univ. Oviedo, Avda. Calvo Sotelo s/n, 33007 Oviedo, Spain

[35] Department of Physics, University of Oxford, Keble Road, Oxford OX1 3RH, UK
[36] Dipartimento di Fisica, Università di Padova and INFN, Via Marzolo 8, 35131 Padua, Italy
[37] Rutherford Appleton Laboratory, Chilton, Didcot OX11 OQX, UK
[38] Dipartimento di Fisica, Università di Roma II and INFN, Tor Vergata, 00173 Rome, Italy
[39] Dipartimento di Fisica, Università di Roma III and INFN, Via della Vasca Navale 84, 00146 Rome, Italy
[40] DAPNIA/Service de Physique des Particules, CEA-Saclay, 91191 Gif-sur-Yvette Cedex, France
[41] Instituto de Fisica de Cantabria (CSIC-UC), Avda. los Castros s/n, 39006 Santander, Spain
[42] Dipartimento di Fisica, Università degli Studi di Roma La Sapienza, Piazzale Aldo Moro 2, 00185 Rome, Italy
[43] Inst. for High Energy Physics, Serpukov P.O. Box 35, Protvino, (Moscow Region), Russian Federation
[44] J. Stefan Institute, Jamova 39, 1000 Ljubljana, Slovenia and Laboratory for Astroparticle Physics, Nova Gorica Polytechnic, Kostanjeviska 16a, 5000 Nova Gorica, Slovenia, and Department of Physics, University of Ljubljana, 1000 Ljubljana, Slovenia
[45] Fysikum, Stockholm University, Box 6730, 113 85 Stockholm, Sweden
[46] Dipartimento di Fisica Sperimentale, Università di Torino and INFN, Via P. Giuria 1, 10125 Turin, Italy
[47] Dipartimento di Fisica, Università di Trieste and INFN, Via A. Valerio 2, 34127 Trieste, Italy and Istituto di Fisica, Università di Udine, 33100 Udine, Italy
[48] Univ. Federal do Rio de Janeiro, C.P. 68528 Cidade Univ., Ilha do Fundão 21945-970 Rio de Janeiro, Brazil
[49] Department of Radiation Sciences, University of Uppsala, P.O. Box 535, 751 21 Uppsala, Sweden
[50] IFIC, Valencia-CSIC, and D.F.A.M.N., U. de Valencia, Avda. Dr. Moliner 50, 46100 Burjassot (Valencia), Spain
[51] Institut für Hochenergiephysik, Österr. Akad. d. Wissensch., Nikolsdorfergasse 18, 1050 Vienna, Austria
[52] Inst. Nuclear Studies and University of Warsaw, Ul. Hoza 69, 00681 Warsaw, Poland
[53] Fachbereich Physik, University of Wuppertal, Postfach 100 127, 42097 Wuppertal, Germany
[54] Now at University of Florida

Received: 5 July 2000 / Revised version: 25 September 2000 /
Published online: 8 December 2000 –

Abstract. Oscillations of B_s^0 mesons have been studied in samples selected from about 3.5 million hadronic Z decays detected by DELPHI between 1992 and 1995. One analysis uses events in the exclusive decay channels: $B_s^0 \to D_s^- \pi^+$ or $D_s^- a_1^+$ and $B_s^0 \to \overline{D}^0 K^- \pi^+$ or $\overline{D}^0 K^- a_1^+$, where the D decays are completely reconstructed. In addition, $B_s^0 - \overline{B_s^0}$ oscillations have been studied in events with an exclusively reconstructed D_s accompanied in the same hemisphere by a high momentum hadron of opposite charge. Combining the two analyses, a limit on the mass difference between the physical B_s^0 states has been obtained:

$$\Delta m_{B_s^0} > 4.0 \text{ ps}^{-1} \text{ at the 95\% C.L.}$$
$$\text{with a sensitivity of } \Delta m_{B_s^0} = 3.2 \text{ ps}^{-1}.$$

Using the latter sample of events, the B_s^0 lifetime has been measured and an upper limit on the decay width difference between the two physical B_s^0 states has been obtained:

$$\tau_{B_s^0} = 1.53^{+0.16}_{-0.15}(\text{stat.}) \pm 0.07(\text{syst.}) \text{ ps}$$

$$\Delta\Gamma_{B_s^0}/\Gamma_{B_s^0} < 0.69 \text{ at the 95\% C.L.}$$

The combination of these results with those obtained using $D_s^\pm \ell^\mp$ sample gives:

$$\Delta m_{B_s^0} > 4.9 \text{ ps}^{-1} \text{ at the 95\% C.L.}$$
$$\text{with a sensitivity of } \Delta m_{B_s^0} = 8.7 \text{ ps}^{-1}.$$

$$\tau_{B_s^0} = 1.46 \pm 0.11 \text{ ps} \quad \text{and} \quad \Delta\Gamma_{B_s^0}/\Gamma_{B_s^0} < 0.45 \text{ at the 95\% C.L.}$$

1 Introduction

In this paper, the average lifetime of the B_s^0 meson is measured and limits are derived on the oscillation frequency of the B_s^0-$\overline{B_s^0}$ system, $\Delta m_{B_s^0}$, and on the decay width difference, $\Delta\Gamma_{B_s^0}$, between mass eigenstates of this system.

Starting with a B_s^0 meson produced at time t=0, the probability, $\mathcal{P}(t)$, to observe a B_s^0 or a $\overline{B_s^0}$ decaying at the proper time t can be written, neglecting effects from CP violation:

$$\mathcal{P}(t) = \frac{\Gamma_{B_s^0}}{2} e^{-\Gamma_{B_s^0} t} \left(\cosh\left(\frac{\Delta\Gamma_{B_s^0}}{2} t \right) \pm \cos(\Delta m_{B_s^0} t) \right) \quad (1)$$

where $\Gamma_{B_s^0} = (\Gamma^H_{B_s^0} + \Gamma^L_{B_s^0})/2$, $\Delta\Gamma_{B_s^0} = \Gamma^L_{B_s^0} - \Gamma^H_{B_s^0}$ and $\Delta m_{B_s^0} = m^H_{B_s^0} - m^L_{B_s^0}$; L and H denote the light and heavy physical states, respectively; $\Delta\Gamma_{B_s^0}$ and $\Delta m_{B_s^0}$ are defined to be positive [1] and the plus (minus) signs in (1) refer to B_s^0 ($\overline{B_s^0}$) decays. The oscillation period gives a direct measurement of the mass difference between the

two physical states. The Standard Model predicts that $\Delta\Gamma_{B_s^0} \ll \Delta m_{B_s^0}$ and the previous expression simplifies to:

$$\mathcal{P}^{unmix}_{B_s^0}(t) \;=\; \Gamma_{B_s^0}\, e^{-\Gamma_{B_s^0} t} \cos^2\left(\frac{\Delta m_{B_s^0} t}{2}\right) \qquad (2)$$

for $B_s^0 \to B_s^0$ and similarly:

$$\mathcal{P}^{mix}_{B_s^0}(t) \;=\; \Gamma_{B_s^0}\, e^{-\Gamma_{B_s^0} t} \sin^2\left(\frac{\Delta m_{B_s^0} t}{2}\right) \qquad (3)$$

for $B_s^0 \to \overline{B_s^0}$. The oscillation frequency, proportional to $\Delta m_{B_s^0}$, can be obtained from the fit of the time distributions given in relations (2) and (3), whereas expression (1), without distinguishing between the B_s^0 and the $\overline{B_s^0}$, can be used to determine the average lifetime and the difference between the lifetimes of the heavy and light mass eigenstates[1].

B physics allows a precise determination of some of the parameters of the CKM matrix. All the nine elements can be expressed in term of 4 parameters that are, in Wolfenstein parameterisation [2], λ, A, ρ and η. The most uncertain parameters are ρ and η.

Several quantities which depend on ρ and η can be measured and, if the Standard Model is correct, they must define compatible values for the two parameters inside measurement errors and theoretical uncertainties. These quantities are ϵ_K, the parameter introduced to measure CP violation in the K system, $|V_{ub}|/|V_{cb}|$, the ratio between the modulus of the CKM matrix elements corresponding to b→u and b→c transitions, and the mass difference $\Delta m_{B_d^0}$.

In the Standard Model, B_q^0-$\overline{B_q^0}$ (q = d, s) mixing is a direct consequence of second order weak interactions. Having kept only the dominant top quark contribution, $\Delta m_{B_q^0}$ can be expressed in terms of Standard Model parameters [3]:

$$\Delta m_{B_q^0} = \frac{G_F^2}{6\pi^2} |V_{tb}|^2 |V_{tq}|^2 m_t^2 m_{B_q} f_{B_q}^2 B_{B_q} \eta_B F(x_t). \qquad (4)$$

In this expression G_F is the Fermi coupling constant; $F(x_t)$, with $x_t = \frac{m_t^2}{m_W^2}$, results from the evaluation of the second order weak "box" diagram responsible for the mixing and has a smooth dependence on x_t; η_B is a QCD correction factor obtained at next-to-leading order in perturbative QCD [4]. The dominant uncertainties in (4) come from the evaluation of the B meson decay constant f_{B_q} and of the "bag" parameter B_{B_q}. The two elements of the V_{CKM} matrix are equal to:

$$|V_{td}| = A\lambda^3\sqrt{(1-\rho)^2+\eta^2}\ , \quad |V_{ts}| = A\lambda^2, \qquad (5)$$

neglecting terms of order $\mathcal{O}(\lambda^4)$.

[1] Throughout the paper the dimension of $\Delta m_{B_s^0}$ will be expressed in ps^{-1} units, because the argument $\Delta m_{B_s^0} t$ in the expression (1) has no dimension. The conversion is given by $ps^{-1} = 6.58 \times 10^{-4} eV/c^2$

In the Wolfenstein parameterisation, $|V_{ts}|$ is independent of ρ and η. A measurement of $\Delta m_{B_s^0}$ is thus a way to measure the value of the non-perturbative QCD parameters.

Direct information on V_{td} can be inferred by measuring $\Delta m_{B_d^0}$. Several experiments have accurately measured $\Delta m_{B_d^0}$, nevertheless this precision cannot be fully exploited to extract information on ρ and η because of the large uncertainty which originates in the evaluation of the non-perturbative QCD parameters.

An efficient constraint is the ratio between the Standard Model expectations for $\Delta m_{B_d^0}$ and $\Delta m_{B_s^0}$, given by:

$$\frac{\Delta m_{B_d^0}}{\Delta m_{B_s^0}} \;=\; \frac{m_{B_d^0} f_{B_d^0}^2 B_{B_d^0} \eta_{B_d^0}}{m_{B_s^0} f_{B_s^0}^2 B_{B_s^0} \eta_{B_s^0}} \frac{|V_{td}|^2}{|V_{ts}|^2}\ . \qquad (6)$$

A measurement of the ratio $\Delta m_{B_d^0}/\Delta m_{B_s^0}$ gives the same type of constraint, in the $\rho-\eta$ plane, as a measurement of $\Delta m_{B_d^0}$, but is expected to be better under control from theory, since the ratios of the decay constants f_{B_q} and of the bag parameters B_{B_q} for B_d^0 and B_s^0 are better known than their individual values [5].

Using existing measurements which constrain ρ and η, except those on $\Delta m_{B_s^0}$, the distribution for the expected values of $\Delta m_{B_s^0}$ can be obtained. It has been shown, for example, in the context of the Electroweak Standard Model and QCD assumptions, that $\Delta m_{B_s^0}$ has to lie, at 68% C.L., between 8 ps^{-1} and 16 ps^{-1} and is expected to be smaller than 21 ps^{-1} at the 95% C.L. [6].

The search for $B_s^0 - \overline{B_s^0}$ oscillations has been the subject of recent intense activity. No signal has been observed so far and the lower limit on the oscillation frequency comes from the combination of the results obtained at LEP, CDF and SLD experiments: $\Delta m_{B_s^0} > 14.3\ ps^{-1}$ at the 95% C.L. [7]. The sensitivity of present measurements is estimated as 14.7 ps^{-1}. These results have been obtained by combining analyses which select various B_s^0 decay channels[2]. Some analyses [8,9] use events containing simply a lepton emitted at large transverse momentum relative to the axis of the jet from which it emerges. In this case, the proper time is measured using an inclusive vertex algorithm to reconstruct the decay distance and the energy of the B hadron candidate. In other analyses, like $D_s^{\pm}\ell^{\mp}$ [10,11], the identified lepton is accompanied, in the same hemisphere, by an exclusively reconstructed D_s. In $D_s^{\pm}h^{\mp}$ analyses (see [12] and the present paper), such leptons are replaced by one or more charged hadrons.

Progress before the next generation accelerators is expected to come from improved analyses of these channels, but the sensitivity at high frequency is essentially limited by the damping of the reconstructed oscillation amplitude due to the limited resolution on the B_s^0 proper time. In general, the proper time resolution σ_t contains two terms and one of them is a time-dependent:

$$\sigma_t = \sqrt{{\sigma_L}^2 + (\sigma_p/p)^2 \times t^2} \qquad (7)$$

[2] Unless explicitly stated otherwise, charge conjugate states are always implied

where σ_L is related to the decay distance resolution, σ_p/p is the relative error on the momentum reconstruction and t is the proper decay time. The damping factor of the oscillation amplitude in this case is given by the following expression [13]:

$$damping = \exp\left(-\left(\Delta m_{B_s^0}\sigma_L\right)^2/2\right)\sqrt{\pi})(\mathrm{x}) \times \exp(\mathrm{x}^2)\mathrm{E}RFC(\mathrm{x}), \quad (8)$$

where x=$1/\sqrt{2}/\Delta m_{B_s^0}$ $1/(\sigma_p/p)$ and ERFC(x)=$2/\sqrt{\pi}$ $\int_x^\infty e^{-t^2}\mathrm{d}t$.

Exclusive (completely reconstructed) decays have a better time resolution for two reasons. As there is no missing particle in the decay, the B_s^0 momentum is known with a good precision and therefore the contribution of the momentum uncertainty to the proper time resolution is negligible. Hence, $\sigma_t = \sigma_L$ and the previous expression is simplified: $damping = \exp(-(\Delta m_{B_s^0}\sigma_L)^2/2)$. In addition, the reconstructed channels are two-body or quasi two-body decays, with an opening angle of their decay products which is on average larger than in multi-body final states; this results in a better accuracy on their decay position determination.

The B_s^0 meson lifetime is expected to be equal to the B_d^0 lifetime [14] within one percent. In the Standard Model, the ratio between the decay width and the mass differences in the B^0-$\overline{B^0}$ system is of the order of $(m_b/m_t)^2$, although large QCD corrections are expected. Explicit calculations to leading order in QCD correction, in the OPE formalism [1] predict:

$$\Delta\Gamma_{B_s^0}/\Gamma_{B_s^0} = 0.16^{+0.11}_{-0.09}$$

where the quoted error is dominated by the uncertainty related to hadronic matrix elements. Recent calculations [15] at next-to-leading order predict a lower value:

$$\Delta\Gamma_{B_s^0}/\Gamma_{B_s^0} = 0.006^{+0.150}_{-0.063}\ .$$

An interesting approach consists in using the ratio between $\Delta\Gamma_{B_s^0}$ and $\Delta m_{B_s^0}$ [15]:

$$\frac{\Delta\Gamma_{B_s^0}}{\Delta m_{B_s^0}} = \left(2.63^{+0.67}_{-1.36}\right)10^{-3}, \quad (9)$$

to constrain the upper part of the $\Delta m_{B_s^0}$ spectrum with an upper limit on $\Delta\Gamma_{B_s^0}/\Gamma_{B_s^0}$. If, in future, the theoretical uncertainty can be reduced, this method can give an alternative way of determining $\Delta m_{B_s^0}$ via $\Delta\Gamma_{B_s^0}$ and, in conjunction with the determination of $\Delta m_{B_d^0}$, can provide an extra constraint on the ρ and η parameters.

After a description of the main features of the DELPHI detector, the event selection and the event simulation in Sect. 2, the two B_s^0 analyses are described. Section 3 presents an analysis of B_s^0-$\overline{B_s^0}$ oscillations from a sample of 44 exclusively reconstructed B_s^0 decays. Section 4 is dedicated to the $D_s^\pm h^\mp$ analysis, in which $B_s^0 \to D_s h X$ decays with fully reconstructed D_s are selected. This analysis also includes a measurement of the B_s^0 meson lifetime and sets a limit on the difference between the decay widths of the physical B_s^0 states, $\Delta\Gamma_{B_s^0}/\Gamma_{B_s^0}$. In Sect. 5 the combined limit on $\Delta m_{B_s^0}$ is given. Finally in Sect. 6, these three results are combined with those obtained using a $D_s^\pm \ell^\mp$ sample [10].

2 The DELPHI detector

The events used in this analysis have been recorded with the DELPHI detector at LEP operating at energies close to the Z peak. The DELPHI detector and its performance were described in detail elsewhere [16]. In this Section, components of the detector and their characteristics, which are the most relevant for these analyses are summarised.

2.1 Charged particle reconstruction

The detector elements used for tracking are the Vertex Detector (VD), the Inner Detector (ID), the Time Projection Chamber (TPC) and the Outer Detector (OD). The VD provides the high precision needed near the primary vertex.

For the data taken from 1991 to 1993, the VD consisted of three cylindrical layers of silicon detectors (at radii of 6.3, 9.0 and 10.9 cm) measuring points in the plane transverse to the beam direction ($r\phi$ coordinate[3]) in the polar angle range between 43° and 137°. In 1994, the first and the third layers were equipped with detector modules with double sided readout, providing a single hit precision of 7.6 μm in $r\phi$, similar to that obtained previously, and 9 μm in z [17]. For high momentum particles with associated hits in the VD, the impact parameter precision close to the interaction region is 20 μm in the $r\phi$ plane and 34 μm in the rz plane. Charged particle tracks are reconstructed with 95% efficiency and with a momentum resolution $\sigma_p/p < 1.5 \times 10^{-3} p$ (p in GeV/c) in the polar angle region between 25° and 155°.

2.2 Hadronic Z selection and event topology

Hadronic events from Z decays were selected by requiring a multiplicity of charged particles greater than four and a total energy of charged particles greater than $0.12\sqrt{s}$, where $\sqrt{s}$ is the centre-of-mass energy and all particles were assumed to be pions; charged particles were required to have a momentum greater than 0.4 GeV/c and a polar angle between 20° and 160°. The overall trigger and selection efficiency is (95.0±0.1)% [18]. A total of 3.5 million hadronic events was obtained from the 1992-1995 data.

Each selected event was divided into two hemispheres separated by the plane transverse to the sphericity axis.

[3] The DELPHI reference frame is defined with z along the e^- beam, x towards the centre of LEP and y upwards. Angular coordinates are θ, measured from z, and the azimuth, ϕ, from the x-axis, while r is the distance from the z-axis

A clustering analysis, based on the JETSET algorithm LUCLUS with default parameters [19], was used to define jets using both charged and neutral particles. These jets were used to compute the p_t^{out} of each particle of the event, as the transverse momentum of this particle with respect to the axis of the jet it belonged to, after having removed this particle from its jet.

2.3 Hadron identification

Hadron identification relied on the RICH detector and on the specific ionisation measurement performed by the TPC.

The RICH detector [16] used two radiators. A gas radiator separated kaons from pions between 3 and 9 GeV/c, where kaons gave no Cherenkov light whereas pions did, and between 9 and 16 GeV/c, using the measured Cherenkov angle. It also provided kaon/proton separation from 8 to 20 GeV/c. A liquid radiator, which has been fully operational since 1994, provided p/K/π separation in the momentum range between 0.7 and 8 GeV/c.

The specific energy loss per unit length (dE/dx) was measured in the TPC by using up to 192 sense wires. At least 30 contributing measurements were required to compute the truncated mean. In the momentum range between 3 and 25 GeV/c, this is fulfilled for 55% of the tracks and the dE/dx measurement has a precision of $\pm 7\%$.

The combination of the two measurements, dE/dx and RICH, provides four levels of pion, kaon and proton tagging [20]: "very loose", "loose", "standard" and "tight" corresponding to different purities. The efficiency and purity of the tagging depend on the momentum of the particle. In the typical momentum range of the B decay products between 2 and 10 GeV/c, the average efficiency (purity) is about 75% (50%) for the "loose", 65% (60%), for the "standard" and 55% (70%) for the "tight" kaon tag. The "very loose" tag indicates that the particle is not identified as a pion. The purity is the proportion of genuine kaons in the selected sample.

Very recently a neural network algorithm has been developed in order to combine the different RICH identification packages optimally. The result of the neural network gives a tagging variable x_{net}, which varies from -1 (pure background) to $+1$ (pure signal). In order to use the same definitions of the kaon tag through all the paper, the "very loose", "loose", "standard" and "tight" tags were defined for a tagging variable x_{net} larger than -0.2, 0.0, 0.4 and 0.6, respectively. This second algorithm has been used in the $D_s^{\pm}h^{\mp}$ analysis (Sect. 4).

2.4 Primary and B vertices reconstruction

The average beam spot position evaluated using the events from different periods of data taking has been used as a constraint in the determination of the e^+e^- interaction point on an event-by-event basis [16]. In 1994 and 1995 data, the position of the primary vertex transverse to the beam is determined with a precision of about 40 μm in the horizontal direction, and about 10 μm in the vertical direction. For 1992 and 1993 data, the uncertainties are larger by about 50%.

For both 1992-1993 and 1994-1995 data, the B decay length was estimated as $L = L_{xy}/\sin\theta_{\rm B}$, where L_{xy} is the measured distance between the primary vertex and the B decay vertex in the plane transverse to the beam direction and $\theta_{\rm B}$ is the polar angle of the B flight direction, estimated from the B decay products. The transverse decay length L_{xy} was given the same sign as the scalar product of the B momentum with the vector joining the primary to the secondary vertex; this procedure gives signed decay length L.

2.5 Λ and K_s^0 reconstruction

The $\Lambda \to p\pi^-$ and $K_s^0 \to \pi^+\pi^-$ decays have been reconstructed using a kinematic fit. The distance in the $r\phi$ plane between the V^0 decay point and the primary vertex was required to be less than 90 cm. This condition meant that the decay products had track segments of at least 20 cm long in the TPC. The reconstruction of the V^0 vertex and selection cuts are described in detail in [16]. Only K_s^0 candidates passing the "tight" selection criteria defined in [16] were retained for this analysis.

2.6 b-tagging

The b-tagging package is described in [21]. The impact parameters of the charged particle tracks, with respect to the primary vertex, were used to build the probability that all tracks come from this vertex. Due to the long B hadron lifetimes, the probability distribution is peaked near zero for events which contain beauty quark whereas it is flat for events containing only light quarks.

2.7 Event simulation

Simulated events were generated using the JETSET 7.3 program [19] with parameters tuned as in [22] and with an updated model of B decay branching fractions. B hadron semileptonic decays were simulated using the ISGW model [23]. Generated events were passed through the full simulation of the DELPHI detector [16], and the resulting simulated raw data were processed through the same reconstruction and analysis programs as the real data.

3 Exclusively reconstructed B_s^0 decays

3.1 Evaluation of B_s^0 branching fractions

For this analysis B_s^0 mesons were reconstructed in $D_s^-\pi^+$, $D_s^-a_1^+$, $\overline{D}^0K^-\pi^+$ and $\overline{D}^0K^-a_1^+$ decay channels. Contributions to the mass spectrum can come also from other decay channels such as $D_s^{*-}\pi^+$, $D_s^{*-}a_1^+$, $\overline{D}^*(2007)^0K^-\pi^+$,

Table 1. Values of the B_s^0 branching fractions used in the current analysis. The notation $\overline{D}^{(*)0}$ defines $\overline{D}^*(2007)^0$ or $\overline{D}^0$ charmed hadrons

B_d^0 decay channel	Measured Br	B_s^0 decay channel	Estimated Br
$B_d^0 \to D^- \pi^+$	$(3.0 \pm 0.4) \times 10^{-3}$	$B_s^0 \to D_s^- \pi^+$	$(3.4 \pm 0.4) \times 10^{-3}$
$B_d^0 \to D^*(2010)^- \pi^+$	$(2.8 \pm 0.2) \times 10^{-3}$	$B_s^0 \to D_s^{*-} \pi^+$	$(3.0 \pm 0.2) \times 10^{-3}$
$B_d^0 \to D^- \rho^+$	$(7.9 \pm 1.4) \times 10^{-3}$	$B_s^0 \to D_s^- \rho^+$	$(9.0 \pm 1.6) \times 10^{-3}$
$B_d^0 \to D^*(2010)^- \rho^+$	$(6.7 \pm 3.3) \times 10^{-3}$	$B_s^0 \to D_s^{*-} \rho^+$	$(6.9 \pm 3.4) \times 10^{-3}$
$B_d^0 \to D^- a_1^+$	$(6.0 \pm 3.3) \times 10^{-3}$	$B_s^0 \to D_s^- a_1^+$	$(6.8 \pm 3.6) \times 10^{-3}$
$B_d^0 \to D^*(2010)^- a_1^+$	$(13.0 \pm 2.7) \times 10^{-3}$	$B_s^0 \to D_s^{*-} a_1^+$	$(13.3 \pm 2.8) \times 10^{-3}$
$B_d^0 \to \overline{D}^{(*)0} \pi^- \pi^+$	see Sect. 3.4	$B_s^0 \to \overline{D}^{(*)0} K^- \pi^+$	$(0.9 \pm 0.5) \times 10^{-3}$
$B_d^0 \to \overline{D}^{(*)0} \pi^- a_1^+$	see Sect. 3.4	$B_s^0 \to \overline{D}^{(*)0} K^- a_1^+$	$(3.0 \pm 1.7) \times 10^{-3}$

$\overline{D}^*(2007)^0 K^- a_1^+$, $D_s^- \rho^+$ and $D_s^{*-} \rho^+$, where the cascade photon or the neutral pion has not been reconstructed. All corresponding branching fractions are unmeasured. An estimation will be used in the following to evaluate the number of the expected B_s^0 events.

To evaluate the two-body $B_s^0 \to D_s^{(*)-} \pi^+ (a_1^+)$ branching fractions, the equivalent decay channels for non-strange mesons were used. This evaluation is based on the numerical application of factorisation done in [24].

For each decay mode of the $B_s^0 \to D_s^{(*)-} M^+$, where M^+ is a π^+ or a ρ^+, the branching fraction is estimated using the following formula:

$$Br\left(B_s^0 \to D_s^{(*)-} M^+\right) = Br^{exp}\left(B_d^0 \to D^{(*)-} M^+\right) \times \frac{Br^{th}\left(B_s^0 \to D_s^{(*)-} M^+\right)}{Br^{th}\left(B_d^0 \to D^{(*)-} M^+\right)}, \quad (10)$$

where the notation $D^{(*)-}$ means $D^*(2010)^-$ or D^- meson. The superscript "exp" designates the experimentally measured values [25], and "th" the predictions from [24]. The theoretical ratios in (10) are close to 1.

For the two-body decays containing D mesons with a_1, the theoretical branching fractions are not available, and the same factors as for the ρ^+ channels have been assumed.

Similar considerations are applied to the three-body decays $B_s^0 \to \overline{D}^0 K^- \pi^+ (a_1^+)$ and $B_s^0 \to \overline{D}^*(2007)^0 K^- \pi^+ (a_1^+)$ using the measurements of $Br(B_d^0 \to \overline{D}^0 \pi^- \pi^+)$ and $Br(B_d^0 \to \overline{D}^0 \pi^- a_1^+)$, which are described in the Sect. 3.4 of the current paper. The ratio of B_s^0 to B_d^0 branching fractions was taken equal to 1.1 (this factor corresponds to the average ratio of the four previous decay modes). Finally, the factor 3.3 was used as the ratio between the B_s^0 decay modes containing a_1^+ and π^+ mesons. This factor was taken as an average between the experimental values for the following B_d^0 two-body decays:

$$\frac{Br(B_d^0 \to D^- a_1^+) + Br(B_d^0 \to D^*(2010)^- a_1^+)}{Br(B_d^0 \to D^- \pi^+) + Br(B_d^0 \to D^*(2010)^- \pi^+)} = 3.3 \pm 0.9 \, .$$

The theoretical calculation [26] gives for this ratio values between 3.4 and 3.5. Table 1 presents the evaluations of several branching fractions of interest for this paper.

3.2 Event sample

Events were selected using the following decay channels:

$B_s^0 \to D_s^- \pi^+$ $\quad D_s^- \to \phi\pi^-, \phi\pi^-\pi^+\pi^-,$ $f(980)\pi^-, K_s^0 K^-, K^{*0} K^-, K^{*0} K^{*-}$

$B_s^0 \to D_s^- a_1^+$ $\quad D_s^- \to \phi\pi^-, K^{*0} K^-$

$B_s^0 \to \overline{D}^0 K^- \pi^+$ $\quad \overline{D}^0 \to K^+\pi^-, K^+\pi^-\pi^+\pi^-$

$B_s^0 \to \overline{D}^0 K^- a_1^+$ $\quad \overline{D}^0 \to K^+\pi^-, K^+\pi^-\pi^+\pi^-$

where the ϕ, K_s^0, f(980), K^{*0}, K^{*-} and a_1 are reconstructed in their charged decay channels: $\phi \to K^+K^-$, $K_s^0 \to \pi^+\pi^-$, $f(980) \to \pi^+\pi^-$, $K^{*0} \to K^+\pi^-$, $K^{*-} \to K_s^0\pi^-$ and $a_1^+ \to \rho^0\pi^+$, $\rho^0 \to \pi^+\pi^-$. D_s and D^0 mesons were reconstructed by considering charged particles in the same hemisphere with at least one VD hit.

D meson candidates were accepted if their mass was within the intervals $1.93 - 2.01$ GeV/c^2 for D_s and $1.83 - 1.90$ GeV/c^2 for D^0. The D decay length was required to be positive and the χ^2–probability of the fitted vertex to be larger than 10^{-5} (10^{-3} for the $D^0 \to K\pi\pi\pi$ decay mode). Different selection criteria were used for different decay channels according to the optimisations derived from dedicated simulated samples. They are described in the following:

- $D_s^- \to \phi\pi^-$. The ϕ meson was reconstructed in the decay mode $\phi \to K^+K^-$ by taking all possible pairs of oppositely charged particles if at least one of them was identified as a "very loose" kaon. The invariant mass of these pairs had to be within ± 12 MeV/c^2 of the nominal ϕ mass value [25]. The momenta of all three particles were required to be larger than 1 GeV/c. In the decay of the D_s meson into a vector (ϕ) and a pseudoscalar meson (π), helicity conservation requires that the angle ψ, measured in the vector meson rest frame between the directions of its decay products and of the pseudoscalar meson, has a $\cos^2\psi$ distribution. The value of $|\cos\psi|$ was required to be larger than 0.3.

• $D_s^- \to \phi\pi^-\pi^+\pi^-$. The ϕ meson was reconstructed as in the previous channel. The momenta of all three pions had to be larger than 0.6 GeV/c.

• $D_s^- \to f(980)\pi^-$. The f(980) meson was reconstructed in the decay mode f(980) $\to \pi^+\pi^-$ by taking all possible pairs of oppositely charged particles classified as pions. This channel suffers from a large combinatorial background which was reduced by selecting candidates having an invariant $\pi^+\pi^-$ mass within 15 MeV/c^2 of the nominal f(980) mass [25] and a total momentum larger than 8 GeV/c. The momenta of all three pions had to be larger than 1 GeV/c.

• $D_s^- \to K_s^0K^-$. K_s^0 meson reconstruction has been described in Sect. 2.5. In addition, the decay length of K_s^0 candidates had to be positive and their momentum to be larger than 2.5 GeV/c. The momentum of the K^- candidate, identified as a "very loose" kaon, had to be larger than 1 GeV/c.

• $D_s^- \longrightarrow K^{*0}K^-$. The K^{*0} meson was reconstructed in the charged decay mode $K^{*0} \to K^+\pi^-$. The K^+ candidate was required to be identified as a "very loose" kaon. The momenta of both particles had to be larger than 1 GeV/c and the invariant mass of the pair had to be within ± 40 MeV/c^2 of the nominal K^{*0} mass [25]. The value of $|\cos\psi|$ (see the $D_s^- \to \phi\pi^-$ selection) had to be larger than 0.3. For the K^- candidate, the combinatorial background is higher than for the kaon coming from K^{*0} resonance. The momentum of the K^- candidate from D_s^- had to exceed 2.5 GeV/c and it had to be identified as a "loose" kaon.

• $D_s^- \longrightarrow K^{*0}K^{*-}$. The K^{*0} meson was reconstructed as previously, but with an invariant mass within ± 60 MeV/c^2 of the nominal K^{*0} mass [25]. This mass interval was chosen larger than in the previous K^{*0} selection, because of the additional constraint from the K^{*-} mass. The K^{*-} meson was reconstructed in the decay mode $K^{*-} \to K_s^0\pi^-$. The K_s^0 meson reconstruction was discussed previously. The invariant mass of K^{*-} candidates had to be within ± 60 MeV/c^2 of the nominal K^{*-} mass [25].

• $\overline{D}^0 \to K^+\pi^-$, $\overline{D}^0 \to K^+\pi^-\pi^+\pi^-$. The $\overline{D}^0$ meson decay to $K^+\pi^-$ has been reconstructed by combining a kaon candidate, identified with the "loose" tag, with an oppositely charged pion with momentum larger than 1 GeV/c. The $\overline{D}^0$ meson decay to $K^+\pi^-\pi^+\pi^-$ has been reconstructed by combining a kaon candidate, identified with the "standard" tag, with three pions, each of them having a momentum larger than 0.5 GeV/c. In order to reduce the combinatorial background, for both decay modes, the kaon momentum was required to be larger than 2.5 GeV/c and the $\overline{D}^0$ momentum candidate to be larger than 10 GeV/c.

Selected $\overline{D}^0$ and D_s^- mesons were used to reconstruct B_s^0 candidates by fitting a common vertex for the $D_s^-\pi^+$, $D_s^-a_1^+$, $\overline{D}^0K^-\pi^+$ or $\overline{D}^0K^-a_1^+$ systems. The π momentum had to be larger than 4 GeV/c. The a_1 candidates were reconstructed using the combination of three pions with momenta larger than 0.8 GeV/c and with an invariant mass situated within the interval 0.95-1.50 GeV/c^2. At least one of the two $\pi^+\pi^-$ combinations was required to have an invariant mass lying within ± 150 MeV/c^2 of the nominal ρ mass [25]. The a_1 momentum had to be larger than 5 GeV/c (6 GeV/c for the $\overline{D}^0 \to K^+\pi^-\pi^+\pi^+$ channel). For all candidates, the $\overline{D}^0$ and D_s^- meson decay distance, relative to the B vertex had to be positive. Events with an estimated error on the B_s^0 decay distance larger than 250 μm and those having a vertex χ^2–probability smaller than 10^{-3} were removed. In order to reduce the combinatorial background from charm and light quarks, the b-tagging probability for the whole event and for the hemisphere opposite to the reconstructed B meson had to be smaller than 0.1. Additional selections which depend on the B_s^0 decay channel were applied, mainly for $\overline{D}^0$ decays which suffer from a larger combinatorial background than D_s^- candidates:

• $B_s^0 \to D_s^-\pi^+$, $B_s^0 \to D_s^-a_1^+$. The momentum of the B_s^0 had to be larger than 22 GeV/c. For $B_s^0 \to D_s^-a_1^+$ candidates, only the combination with the largest B_s^0 momentum has been kept.

• $B_s^0 \to \overline{D}^0K^-\pi^+$, $B_s^0 \to \overline{D}^0K^-a_1^+$. For $B_s^0 \to \overline{D}^0K^-\pi^+$ decays, the B_s^0 momentum had to be larger than 27 GeV/c. Because of a high combinatorial background for $B_s^0 \to \overline{D}^0K^-a_1^+$ decays, the B_s^0 momentum had to be larger than 29 GeV/c in the $\overline{D}^0 \to K^+\pi^-$ channel and larger than 33 GeV/c in the $\overline{D}^0 \to K^+\pi^-\pi^+\pi^-$ decay channel. In each event, only the candidate with the largest B_s^0 momentum was kept. For the K^- candidate, identified as "standard", the momentum had to be larger than 2 GeV/c. The source of the $\overline{D}^0$ and K^- meson pair can be an excited D meson state. The constraint on the mass value of such a state allows more soft K^- mesons to be considered. The selection on the K^- momentum was reduced to 1.5 GeV/c, if the invariant mass of the $\overline{D}^0K^-$ pair was compatible with the mass of the orbitally excited $D_{sJ}(2573)$ state (the most probable value of J is 2 [25]). One event was detected, which is compatible with the decay channel $B_s^0 \to D_{sJ}(2573)^-\pi^+$, $D_{sJ}(2573)^- \to \overline{D}^0K^-$: the momentum of the K^- candidate is 1.8 GeV/c and the mass difference $M(\overline{D}^0K^-) - M(\overline{D}^0)$ is 716.0 ± 2.1 MeV/c^2. The expected mass difference of 708.9 ± 1.8 MeV/c^2 is in good agreement with the observed one, taking into ac-

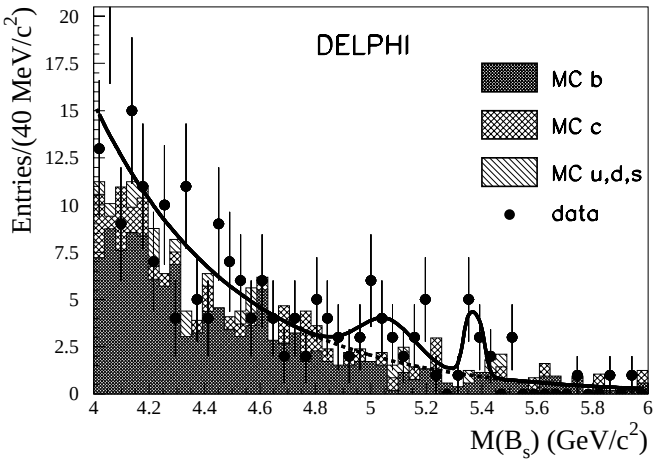

Fig. 1. B_s^0 mass spectrum for the candidates selected in the twelve decay channels described in Sect. 3.2. The data are indicated by the points with error bars and the result of the fit has been superimposed. Details on this fit are given in the text. The histograms represent the expected contribution from beauty events (after having removed the exclusively reconstructed B_s^0 decay channels), from charm events and from light quark events

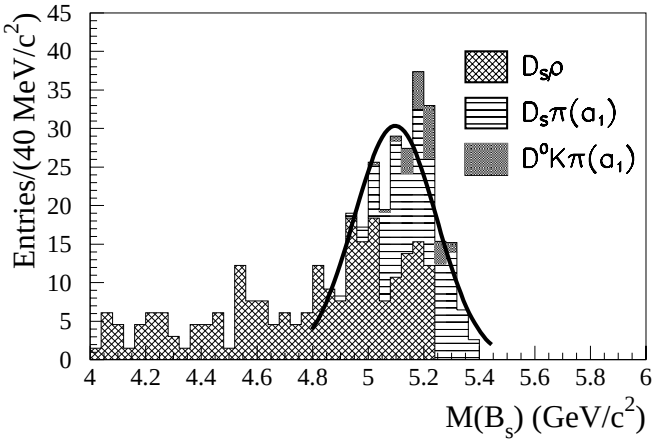

Fig. 2. The Monte Carlo composition of the satellite peak including the effects of experimental resolution. The notations in the plot are the following: $D_s\rho$ corresponds to $D_s^-\rho^+$ and $D_s^{*-}\rho^+$ decay channels of the B_s^0; $D_s\pi(a_1)$ corresponds to $D_s^{*-}\pi^+$ and $D_s^{*-}a_1^+$; $D^0K\pi(a_1)$ shows the contribution from $\overline{D}^*(2007)^0K^-\pi^+$ and $\overline{D}^*(2007)^0K^-a_1^+$ decay channels. All contributions have been normalised according to the evaluation of the branching fractions discussed in Sect. 3.1 and including reconstruction efficiencies evaluated using simulated events

count the full width of this state which is 15^{+5}_{-4} MeV/c^2 [25].

The mass spectrum, obtained by summing up the contributions from the different channels is shown in Fig. 1. The data are indicated by points with error bars and the fit result is shown by the solid line. The mass distribution in the signal region was fitted using two Gaussian functions of different widths to account for the exclusive B_s^0 signal (main narrow peak) and for the presence of partially reconstructed B_s^0 decays (satellite wider peak). According to the expected branching fractions, it was assumed that the dominant contributions for the satellite peak come from the following decay channels: $D_s^{*-}\pi^+$, $D_s^{*-}a_1^+$, $\overline{D}^*(2007)^0K^-\pi^+$, $\overline{D}^*(2007)^0K^-a_1^+$, $D_s^-\rho^+$ and $D_s^{*-}\rho^+$, where the cascade photon or neutral pion (or both) were not reconstructed. In the simulation, it was verified that the mass distribution of the satellite peak can be described by a Gaussian function as shown in Fig. 2. The central values and the widths of the Gaussian functions (main and satellite peaks) in Fig. 1 were left free to vary in the fit. The combinatorial background was fitted using an exponential function with a slope fixed according to the simulation. This slope was verified in several ways. Using 2.9 million $b\bar{b}$ and 5.3 million $q\bar{q}$ simulated events, the expected mass spectrum was obtained after having removed the B_s^0 signal contribution in the mass region of the satellite and main peaks. The sum of the contributions from b events, charm events and light-quark events is shown in Fig. 1 and is in agreement with that obtained in data. Two further checks were performed, using events selected in the side-bands of the D_s^- and $\overline{D}^0$ candidates and from wrong sign combinations. The slopes of both distributions are in agreement with those obtained by fitting the data and the simulation.

The fit to the mass distribution yielded a signal of 8 ± 4 B_s^0 decays in the main peak and 15 ± 8 events in the satellite peak. The probability that the background has fluctuated to give the observed number of events in the main peak is 3×10^{-4}. Table 2 gives the characteristics of the observed signals and the comparison with simulation. Specific decay channels from B_s^0, B_d^0, B^+ and $\overline{\Lambda_b^0}$ were simulated with statistics ranging from ten to several thousand times the expected rates in real data. These samples were used to determine efficiencies and reflection probabilities discussed below.

3.3 Reflections from B_d^0 and $\overline{\Lambda_b^0}$ decays

For several B_s^0 decay channels a possible physical background originates from non-strange B decays, when one of the pions or proton is misidentified as a kaon (kinematic reflections). The main decay channels are $B_d^0 \to D^-\pi^+(a_1^+)$, $D^- \to K^{*0}\pi^-$ (which can contribute to $B_s^0 \to D_s^-\pi^+(a_1^+)$, $D_s^- \to K^{*0}K^-$ candidates) and from $B_d^0 \to \overline{D}^0\pi^-\pi^+$, $\overline{D}^0 \to K^+\pi^-$ or $K^+\pi^-\pi^+\pi^-$ (which can contribute to $B_s^0 \to \overline{D}^0K^-\pi^+$ candidates). In the mass region of the main peak, 0.32 ± 0.13 events are expected to originate from kinematic reflections (with a 19% contribution from $\overline{\Lambda_b^0}$ decays). These estimates were obtained using dedicated Monte Carlo samples of B_d^0 and $\overline{\Lambda_b^0}$ events passed through the full reconstruction algorithms and satisfying the selection criteria. The corresponding uncertainties come from the limited knowledge of the assumed branching fractions and from the simulated events statistics.

To study the contribution in the satellite peak from kinematic reflections, the same decay processes were con-

Table 2. Characteristics of the B_s^0 signals and comparison with the simulation. The expected numbers of events were calculated taking into account the different branching fractions as given in Table 1 and the corresponding reconstruction efficiencies. These efficiencies vary from $(0.2 \pm 0.1)\%$ for the $B_s^0 \to \overline{D}^0 K^- a_1^+$ with $\overline{D}^0 \to K^+\pi^-\pi^+\pi^-$, up to $(10.2 \pm 0.8)\%$ for the $B_s^0 \to D_s^- \pi^+$ with $D_s^- \to \phi\pi^-$. The fitted or expected number of signal events and the fraction of combinatorial background are given inside a mass window corresponding to $\pm 3\sigma(\pm 2\sigma)$ for the main(satellite) peaks. In real data the number of events in these mass windows are 11(33). The B_s^0 mass in the simulation is 5.370 GeV/c^2. In the last column the fraction of physical background, discussed in detail in Sect. 3.3, is given

Data set	Mass (GeV/c^2)	Width (σ) (GeV/c^2)	N_{signal}	Comb. bkg %	Reflection %
Main peak					
Real Data	5.373 ± 0.016	0.029 ± 0.012	8 ± 4	27 ± 16	-
Simulation	5.370 ± 0.002	0.037 ± 0.002	5 ± 1	-	7 ± 3
Satellite peak					
Real Data	5.050 ± 0.054	0.111 ± 0.049	15 ± 8	55 ± 13	-
Simulation	5.099 ± 0.007	0.148 ± 0.007	11 ± 2	-	12 ± 6

sidered with channels in which the D meson is accompanied by a ρ. This gives 1.3 ± 0.7 events.

In order to look for possible signals coming from kinematic reflections in real data, B_s^0 candidates were considered in turn as B_d^0 or $\overline{\Lambda_b^0}$ hadrons by changing the kaon into a pion or an antiproton, respectively. The mass distributions obtained are similar to those expected from genuine simulated B_s^0 mesons and do not show any accumulation of events in the B_d^0 or $\overline{\Lambda_b^0}$ mass regions.

3.4 Reconstruction of non-strange B meson decays

Non-strange B mesons, decaying into a $\overline{D}^0$ and a small number of pions, were reconstructed in order to verify the B_s^0 reconstruction algorithms. The $B^+ \to \overline{D}^0\pi^+$, $B_d^0 \to D^*(2010)^-\pi^+$ and $B_d^0 \to D^*(2010)^- a_1^+$ decay channels were studied and their mass distributions are shown in Figs. 3a and 3b. They were fitted using a Gaussian function for the signal and using an exponential function for the combinatorial background. An additional Gaussian function was used in Fig. 3a to account for the signal coming from the following decay channels: $B^+ \to \overline{D}^*(2007)^0\pi^+$, $B^+ \to \overline{D}^0\rho^+$, $B^+ \to \overline{D}^*(2007)^0\rho^+$, where the π^0 and/or γ from the $\overline{D}^*(2007)^0$ and/or ρ decays were not reconstructed. The main selection criteria which were imposed are rather similar to those used in the B_s^0 analysis. The information relevant to these reconstructed channels is given in Table 3. The numbers of observed events are in agreement with expectations.

Finally two B_d^0 decay channels, $B_d^0 \to \overline{D}^0\pi^-\pi^+$ and $B_d^0 \to \overline{D}^0\pi^- a_1^+$ which are not yet well established, were considered.

In the strange B sector (Sect. 3.1) they correspond to the $B_s^0 \to \overline{D}^0 K^-\pi^+$ and $B_s^0 \to \overline{D}^0 K^- a_1^+$ decays. B_d^0 mesons were reconstructed using the same selection criteria as for the corresponding B_s^0 decay channel, but replacing a K meson by a π. All particles, not explicitly identified as protons or kaons were accepted as pions. In order to remove the $B_d^0 \to D^*(2010)^-\pi^+$ and $B_d^0 \to D^*(2010)^- a_1^+$ contamination, candidates were required to have a mass difference $M(\overline{D}^0\pi^-) - M(\overline{D}^0)$ larger than 0.16 GeV/c^2.

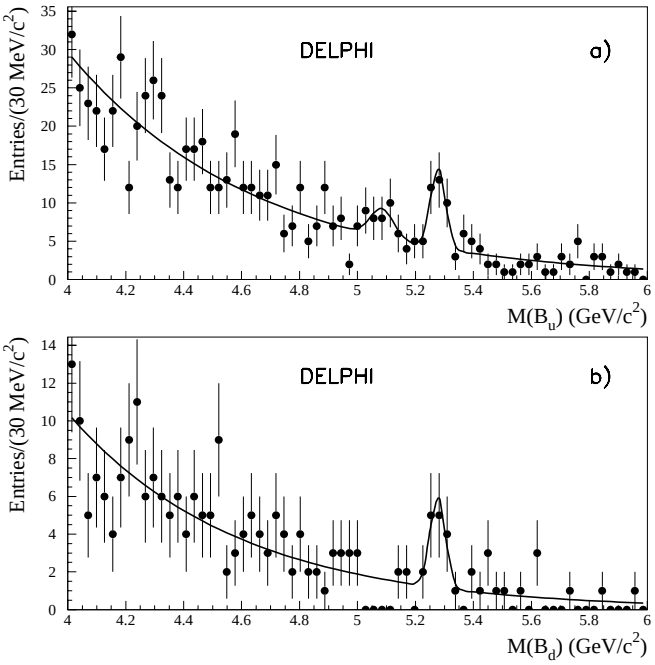

Fig. 3a,b. Mass spectra for **a** $B^+ \to \overline{D}^0\pi^+$, **b** $B_d^0 \to D^*(2010)^-\pi^+$ and $B_d^0 \to D^*(2010)^- a_1^+$ decays. In the first plot a signal from $B^+ \to D^*(2007)^0\pi^+$, $B^+ \to \overline{D}^0\rho^+$ and $B^+ \to \overline{D}^*(2007)^0\rho^+$ (satellite peak) is also visible. Details on the fit are given in the text

Table 3. Characteristics of the non-strange B decay mode and comparison with the simulation. The error on the expected number of events comes from the errors in the branching fractions and reconstruction efficiencies. The branching fraction of the decay mode in the last row is estimated in this paper

Channel	B meson mass (GeV/c^2)	N_{obs}	N_{exp}
$B^+ \to \overline{D}^0\pi^+$	5.278 ± 0.008	24 ± 5	28 ± 5
$B_d^0 \to D^*(2010)^-\pi^+ + D^*(2010)^-a_1^+$	5.277 ± 0.011	11 ± 5	10 ± 4
$B_d^0 \to \overline{D}^0\pi^-\pi^+ + \overline{D}^0\pi^-a_1^+$	5.287 ± 0.024	8 ± 4	–

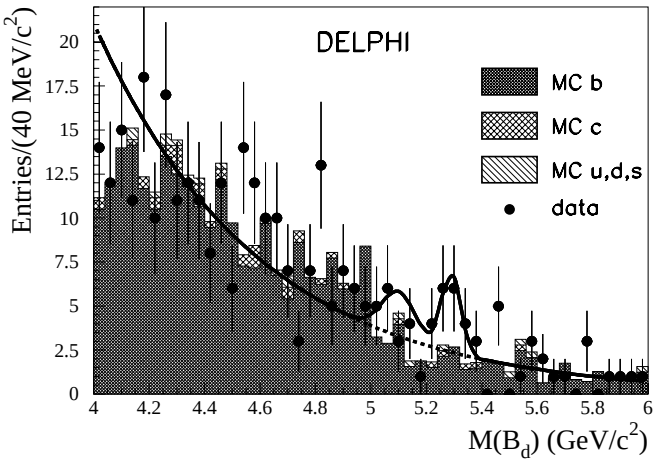

Fig. 4. B_d^0 mass spectrum for the sum of $B_d^0 \to \overline{D}^0\pi^-\pi^+$ and $B_d^0 \to \overline{D}^0\pi^-a_1^+$ decays selected in the four decay channels described in Sect. 3.4. The data are indicated by the points with error bars and the result of the fit has been superimposed. The histograms represent the expected contribution from beauty events (after having removed the exclusively reconstructed B_d^0 decay channels), from charm events and from light quark events. The widths of the signals have been fixed according to the values found in the simulation. Details on the fit are given in the text

Figure 4 shows the mass distribution for these two decay channels. It was fitted with an exponential function for the background and two Gaussian functions for the signals corresponding to the main and satellite peaks, with respective widths equal to about 34 MeV/c^2 and 60 MeV/c^2, as obtained from the simulation. The position of the wider Gaussian, corresponding to $B_d^0 \to \overline{D}^*(2007)^0\pi^-\pi^+$ and $B_d^0 \to \overline{D}^*(2007)^0\pi^-a_1^+$ signals with unreconstructed π^0 or γ, and the slope of the background exponential function were also taken from the simulation. The fit to the mass distribution yielded a signal of 8 ± 4 B_d^0 decays in the main peak. The probability that the background has fluctuated to give the observed number of events is 3×10^{-2}.

The number of observed events in the main peak can be translated into a branching fraction: $Br(B_d^0 \to \overline{D}^0\pi^-\pi^+ + \overline{D}^0\pi^-a_1^+) = (3.6 \pm 1.9) \times 10^{-3}$. The quoted error is completely dominated by statistics. The CLEO Collaboration has given an upper limit [25] only on the decay channel with a pion pair: $Br(B_d^0 \to \overline{D}^0\pi^-\pi^+) < 1.6\times10^{-3}$ (at the 90% C.L.). This limit is consistent with those which can be extracted from the measured channels in this paper:

$$Br(B_d^0 \to \overline{D}^0\pi^-\pi^+) < 1.6 \times 10^{-3} \text{ at the 90\% C.L.}$$
$$Br(B_d^0 \to \overline{D}^0\pi^-a_1{}^+) < 5.4 \times 10^{-3} \text{ at the 90\% C.L.}$$

For this evaluation it was assumed (see Sect. 3.1) that the decay channel with a_1^+ is produced with a rate which is (3.3 ± 0.9) times larger than the channel with π^+.

3.5 Study of B_s^0-$\overline{B_s^0}$ oscillations

3.5.1 Algorithm for tagging b or $\overline{b}$ quark at production time

The signature of the initial production of a b ($\overline{b}$) quark in the jet containing the B_s^0 or $\overline{B_s^0}$ candidate was determined using a combination of different variables sensitive to the initial quark state. For each individual variable X_i, the probability density functions $f_b(X_i)$ ($f_{\overline{b}}(X_i)$) for b ($\overline{b}$) quarks were built and the ratio $R_i = f_{\overline{b}}(X_i)/f_b(X_i)$ was computed. The combined tagging variable is defined as:

$$x_{tag} = \frac{1-R}{1+R} \text{ , where } R = \prod R_i. \qquad (11)$$

The variable x_{tag} varies between -1 and 1. Large and positive values of x_{tag} correspond to a high probability that the produced quark is a b rather than a $\overline{b}$ in a given hemisphere.

A set of nine discriminant variables has been selected for this analysis. One set (three variables) is determined in the hemisphere which contains the B_s^0 meson, the other set (five variables) in the hemisphere opposite to the B_s^0 meson, and one variable is common to both hemispheres. Details concerning the definition of these variables and the method are given in [10].

An event was classified as a mixed or as an unmixed candidate according to the sign, Q_D, of the D_s electric charge for decay channels containing a D_s meson, or according to the sign of the kaon for $\overline{D}^0K^-\pi^+$ decay channels, relative to the sign of the x_{tag} variable. Mixed candidates are defined by requiring $x_{tag} \cdot Q_D < 0$, and unmixed candidates correspond to $x_{tag} \cdot Q_D > 0$. The probability, ϵ_b^{tag}, for tagging correctly the b or $\overline{b}$ quark, from the measurement of x_{tag}, was evaluated by using a dedicated simulated event sample and was found to be (74.5±0.5)%.

Table 4. Proper time resolution from simulation for 1992-1993 and 1994-1995 data sets and for the different decay channels. It has been parameterised by the sum of two Gaussian functions

Main peak				
Decay channels	Years	σ_1(ps)	σ_2(ps)	f_2
all B_s^0 channels	1992-1993	0.068	0.18	0.27
all B_s^0 channels	1994-1995	0.065	0.12	0.42
Satellite peak				
$D_s^{*-}\pi^+(a_1^+)$, $\overline{D}^*(2007)^0K^-\pi^+(a_1^+)$	1992-1993	0.066	0.15	0.48
$D_s^{*-}\pi^+(a_1^+)$, $\overline{D}^*(2007)^0K^-\pi^+(a_1^+)$	1994-1995	0.081	0.17	0.30
$D_s^-\rho^+$, $D_s^{*-}\rho^+$	1992-1993	0.085	0.21	0.65
$D_s^-\rho^+$, $D_s^{*-}\rho^+$	1994-1995	0.092	0.20	0.57

The corresponding probability for events in the combinatorial background was obtained using real data candidates selected in the side-bands of the D signal: the probabilities to classify these events as mixed or unmixed candidates are called ϵ_{comb}^{mix} and ϵ_{comb}^{unmix}, respectively. For the reflection events the analogous probabilities are called ϵ_{ref}^{mix}, ϵ_{ref}^{unmix} and their values were taken from the simulation.

3.5.2 Proper time resolution

For each event, the B_s^0 proper decay time was obtained from the measured decay length ($L_{B_s^0}$) and the estimate of the B_s^0 momentum ($p_{B_s^0}$). The measured position of the D_s^- or $\overline{D}^0$ decay vertex, the momentum, and the corresponding measurement errors, were used to reconstruct a D_s^- or a $\overline{D}^0$ particle. A candidate B_s^0 decay vertex was obtained by intercepting the trajectory of this particle with the other charged particle tracks which are supposed to come from the B_s^0 decay vertex.

For the main peak, the B_s^0 momentum is precisely known since all decay products are reconstructed. For the satellite peak, this is no longer true, because there are one or two undetected neutral(s) (π^0 and/or γ) in the B_s^0 decay. As discussed in Sect. 3.2, the satellite peak is assumed to be composed of $D_s^{*-}\pi^+$, $D_s^{*-}a_1^+$, $D_s^-\rho^+$, $D_s^{*-}\rho^+$ and $\overline{D}^*(2007)^0K^-\pi^+$, $\overline{D}^*(2007)^0K^-a_1^+$ decays. The first four decay channels give $D_s^-\pi^+(a_1^+)$ and the last two channels give $\overline{D}^0K^-\pi^+(a_1^+)$ final states. Kinematic mass constrained fits (imposing the mass of B_s^0 and of the intermediate states with corresponding errors) were performed assuming always the presence of a γ coming from the D_s^{*-} or $\overline{D}^*(2007)^0$ meson decays. This is a good approximation also for decay channels containing a ρ^+ meson. These mass constrained fits were performed on events lying in the mass region corresponding to $\pm 2\sigma$ of the fitted mass of the satellite peak.

Except for the combinatorial background contribution, the predicted proper time distributions were obtained by convoluting the theoretical functions with resolution functions evaluated from simulated events. Due to the different decay length resolutions (for the different Vertex Detector configurations), proper time resolutions were used for data samples taken in 1992-1993 and 1994-1995 separately. The proper time resolution, $\mathcal{R}_{B_s}(t-t_i)$, was evaluated from the difference between the generated time (t) and the reconstructed time (t_i), fitting this distribution by the sum of two Gaussian functions:

$$\mathcal{R}_{B_s}(t-t_i) = (1-f_2)G_1(t-t_i,\sigma_1) + f_2 G_2(t-t_i,\sigma_2) \quad (12)$$

where $G_1(t-t_i,\sigma_1)$ and $G_2(t-t_i,\sigma_2)$ are Gaussian functions with the corresponding resolutions σ_1 and σ_2. In the general case, the σ_i resolutions depend on the momentum uncertainty (see (1)). But in this analysis, as the B_s^0 momentum is known with a good precision, the contribution of the momentum uncertainty to the proper time resolution is negligible. f_2 is the fraction of the second Gaussian function, which, by convention, is that with the worse resolution. The values of the corresponding parameters, obtained from simulated events, are given in Table 4. The time resolution for events in the satellite peak is only slightly worse than for those belonging to the main peak.

The time distribution $\mathcal{P}_{comb}(t_i)$ for the combinatorial background under the main peak is obtained from real data by fitting the time distribution of wrong-sign and right-sign events lying in the side-bands of the B_s^0 mass distribution. It was verified, in the simulation, that the time distribution for these classes of events is similar to that obtained for events lying under the B_s^0 mass peak. The time distribution $\mathcal{P}_{comb}(t_i)$ for the combinatorial background under the satellite peak was taken directly from the simulation, since it has a dependence on the measured B_s^0 mass, due to the procedure used to reconstruct the B momentum for these events. The time distribution $\mathcal{P}_{ref}(t_i)$ for the reflection was also taken from the simulation.

3.5.3 Fitting procedure

The oscillation analysis is performed in the framework of the amplitude method [13], which consists in measuring, for each value of the frequency $\Delta m_{B_s^0}$, an amplitude A

and its error $\sigma(A)$. The parameter A is introduced in the time evolution of pure B_s^0 or $\overline{B}_s^0$ states, so that the value $A = 1$ corresponds to a genuine signal for oscillation. The time-dependent probability that B_s^0 is detected as a B_s^0 or $\overline{B}_s^0$ is then:

$$\mathcal{P}^{unmix(mix)}(t) = \frac{1}{2\tau_{B_s^0}} \times \exp(-t/\tau_{B_s^0}) \times(1 \pm A\ \cos(\Delta m_{B_s^0} t)) \qquad (13)$$

where the plus (minus) signs refer to B_s^0 ($\overline{B_s^0}$) decays. The 95% C.L. excluded region for $\Delta m_{B_s^0}$ is obtained by evaluating the probability that, in at most 5% of the cases, a real signal having an amplitude equal to unity would give an observed amplitude smaller than the one measured. This corresponds to the condition:

$$A(\Delta m_{B_s^0}) + 1.645\ \sigma(A(\Delta m_{B_s^0}))\ <\ 1.$$

In the amplitude approach, the error $\sigma(A(\Delta m_{B_s^0}))$ is related to the probability to exclude a given value of $\Delta m_{B_s^0}$. The sensitivity is defined as the value of $\Delta m_{B_s^0}$ which would just be excluded, if the value of A, as measured in the experiment, was zero for all values of $\Delta m_{B_s^0}$, i.e. it is the expected 95% confidence limit that an experiment of the same statistics and resolution would be expected to achieve (a real experiment would set a higher or lower limit, because of fluctuations in the values of A as a function of $\Delta m_{B_s^0}$).

The probability distributions for mixed and unmixed[4] events are:

$$P^{mix}(t_i) = f_{B_s} P^{mix}_{B_s}(t_i) + f_{ref} P^{mix}_{ref}(t_i) + f_{comb} P^{mix}_{comb}(t_i) \qquad (14)$$

where f_{B_s}, f_{ref} and f_{comb} are the relative fractions of the B_s^0, reflection and combinatorial background events, respectively, which satisfy the condition $f_{B_s}+f_{ref}+f_{comb}=1$. The expressions for the different probability densities are:

– B_s^0 mixing probability:

$$P^{mix}_{B_s}(t_i) = \{\ \epsilon_b^{tag} \mathcal{P}^{mix}_{B_s}(t) + (1-\epsilon_b^{tag}) \mathcal{P}^{unmix}_{B_s}(t)\ \} \otimes \mathcal{R}_{B_s}(t - t_i) \qquad (15)$$

– Reflection mixing probability:

$$P^{mix}_{ref}(t_i) = \epsilon^{mix}_{ref} \mathcal{P}_{ref}(t_i) \qquad (16)$$

– Combinatorial background mixing probability:

$$P^{mix}_{comb}(t_i) = \epsilon^{mix}_{comb} \mathcal{P}_{comb}(t_i) \qquad (17)$$

The parameters ϵ_b^{tag}, ϵ^{mix}_{ref} and ϵ^{mix}_{comb} were defined in Sect. 3.5.1.

[4] In the following, only the probability distribution for mixed events is written explicitly; the corresponding probability for unmixed events can be obtained by changing ϵ into $(1-\epsilon)$

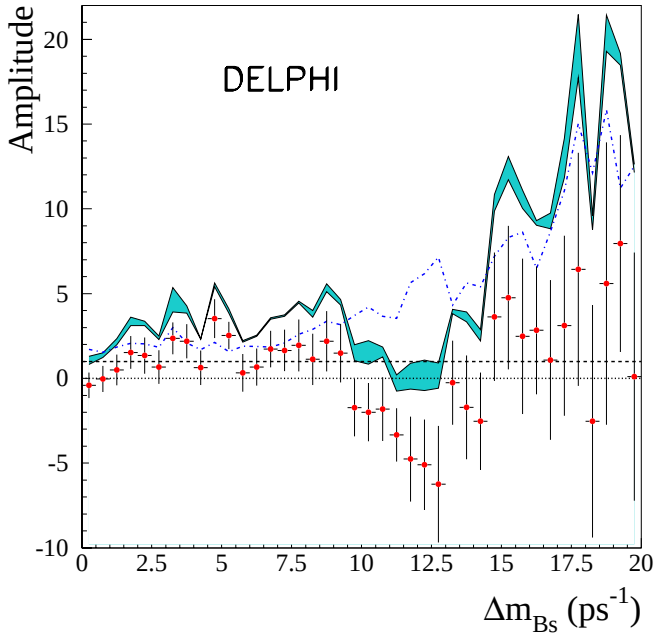

Fig. 5. Exclusive B_s^0 analysis: variation of the oscillation amplitude A as a function of $\Delta m_{B_s^0}$. The lower continuous line corresponds to $A + 1.645\ \sigma(A)$ where $\sigma(A)$ includes statistical uncertainties only, while the shaded area shows the contribution from systematics. The dashed-dotted line corresponds to the sensitivity curve. The lines at A=0 and A=1 are also given.The points with error bars are real data

The amplitude analysis is then performed using all events selected in a mass region between 4.83 and 5.46 GeV/c^2. The variation of the background level as a function of the reconstructed mass was included in this analysis on an event-by-event basis. Figure 5 shows the variation of the measured amplitude as a function of $\Delta m_{B_s^0}$. With the present level of the statistics, this analysis provides a negligible low limit. On the other hand, its most important feature, despite the low statistics, is the relatively small error on the amplitude at high values of $\Delta m_{B_s^0}$ with respect to the more inclusive analyses. Due to the limited statistics, the error on A ($\sigma(A)$) can be asymmetric. The error has been symmetrized by taking the larger value. Figure 6a shows the variation of the measured error on the amplitude as a function of $\Delta m_{B_s^0}$. In Fig. 6b the results from the $D_s^{\pm}\ell^{\mp}$ [10] and from the $D_s^{\pm}h^{\mp}$ (see the second part of the current paper) are compared with the exclusive B_s^0 analysis. It should be noted that, due to the better proper time resolution, the resolution $\sigma(A)$ of the B_s^0 exclusive analysis increases more slowly. The ratio of the corresponding errors of B_s^0 exclusive and $D_s^{\pm}\ell^{\mp}$ analyses is about 5 (2) at the low (high) values of $\Delta m_{B_s^0}$.

The behaviour of $\sigma(A)$ was investigated using a "toy" Monte Carlo generated with the same characteristics as those measured in real data. The individual toy experiments show a similar behaviour of $\sigma(A)$, as in the real data, as a function of $\Delta m_{B_s^0}$. For each value of $\Delta m_{B_s^0}$, the distribution of $\sigma(A)$ and its variance was obtained. The

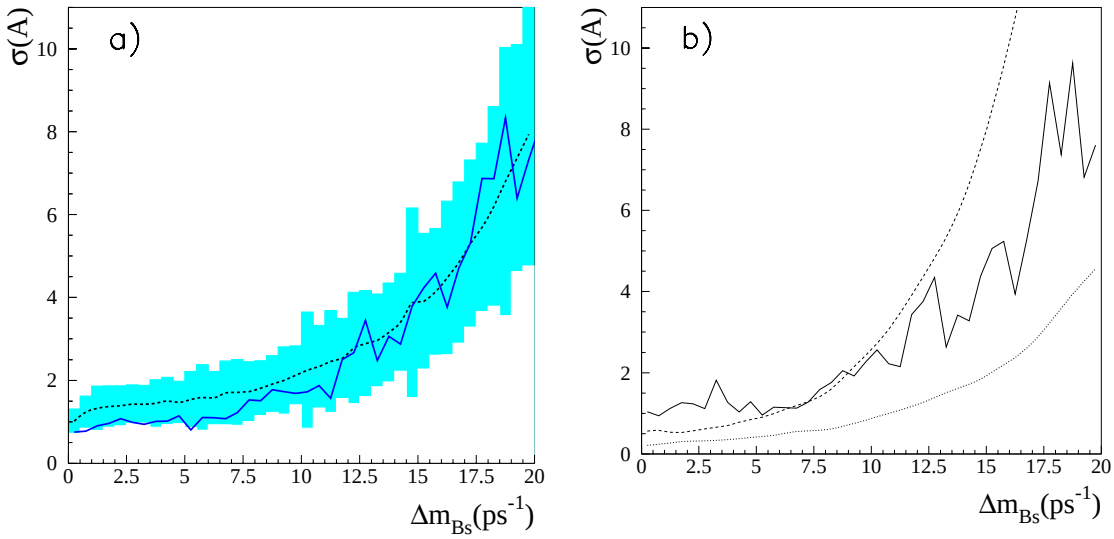

Fig. 6a,b. $\sigma(A)$ as a function of $\Delta m_{B_s^0}$. **a** Exclusive B_s^0 analysis: the full curve shows the result from the data. The dashed curve shows the average result from 100 toy experiments with the same statistics as in data and the shaded area gives the $\pm 2\sigma(A)$ region around this average. The systematic effects are not included. **b** Comparison of the $\sigma(A)$ as function of $\Delta m_{B_s^0}$ for three analyses: the full curve shows the result from the exclusive B_s^0 analysis, the dashed and dotted curves show the result from $D_s^{\pm}h^{\mp}$ and $D_s^{\pm}\ell^{\mp}$ analyses, respectively

central value and the region corresponding to a $\pm 2\sigma(A)$ variation are also shown in Fig. 6a.

3.5.4 Study of systematic uncertainties

Systematic uncertainties were evaluated by varying the parameters, which were kept constant in the fit according to their measured or expected errors.

- Systematics from the tagging purity:
  a variation of ±3% on the expected tagging purity for the signal was considered, following the results given in [10].
- Systematics from the background level and kinematic reflection:
  the levels of background and of kinematic reflection were varied separately for the main peak and for the satellite peak according to the statistical uncertainties given in Table 2. Since the level of the combinatorial background was used as a function of the reconstructed mass on an event-by-event basis, the measured central mass positions and the corresponding widths were also varied by $\pm 1\sigma$ around their fitted values.
- Systematics from the expected resolution on the B decay proper time:
  the widths σ_1 and σ_2 described in Sect. 3.5.2 and given in Table 4 were varied by ±10% [10,27,28].
- Finally, uncertainties in the values of the B_s^0 meson lifetime ($\tau_{B_s^0} = 1.46 \pm 0.06$ ps [7]) and in the parameterisation of the proper time of the combinatorial background were taken into account.

In Fig. 5, which presents the variation of the measured amplitude as a function of $\Delta m_{B_s^0}$, the shaded area shows the contribution from systematics.

4 $D_s^{\pm}h^{\mp}$ analysis with fully reconstructed D_s

Events with an exclusively reconstructed D_s accompanied by one or more large momentum hadrons were used to perform a second oscillation analysis. This channel is similar to the $D_s^{\pm}\ell^{\mp}$ final state [10] but, instead of a charged lepton, it uses charged hadrons. It provides a larger number of events but suffers from an ambiguity in the choice of the hadrons and from a reduced B_s^0 purity of the selected sample. This approach has already been used in DELPHI to measure the B_s^0 lifetime [27].

4.1 Event selection

The D_s meson is selected in two decay channels:

$$D_s^- \to \phi\pi^-, \quad \phi \to K^+K^-;$$
$$D_s^- \to K^{*0}K^-, K^{*0} \to K^+\pi^-.$$

D_s candidates were reconstructed by making combinations of three charged particles located in the same event hemisphere, with a momentum larger than 1 GeV/c and with reconstructed tracks associated to at least one VD hit. The value of $|\cos\psi|$ (see Sect. 3.2) was required to be larger than 0.4 and 0.6 in the $D_s^- \to \phi\pi^-$ and $D_s^- \to K^{*0}K^-$ decay channels, respectively. In order to reduce the combinatorial background from charm and light quarks, the b-tagging probability for the whole event was required to be smaller than 0.5.

In this analysis the neural network algorithm for hadron identification described in Sect. 2.3 was used. For the $D_s^- \to \phi\pi^-$ decay mode, the invariant mass of ϕ candidates was required to be within ±12 MeV/c^2 of the nominal ϕ mass and the ϕ momentum was required to be larger

Table 5. Number of D_s mesons reconstructed in the $\phi\pi^-$ and $K^{*0}K^-$ decay channels after selection of the accompanying hadron(s). The fraction of combinatorial background, given in parentheses, has been evaluated using a mass interval of $\pm 2\sigma$ centred on the fitted D_s mass

D_s decay channels	D_s signal in 1992-1993 data	D_s signal in 1994-1995 data
$D_s^- \to \phi\pi^-$	322 ± 30 (0.60 ± 0.04)	468 ± 42 (0.53 ± 0.04)
$D_s^- \to K^{*0}K^-$	152 ± 28 (0.70 ± 0.06)	324 ± 35 (0.58 ± 0.05)

than 5 GeV/c. If the K^+K^- invariant mass was within ± 4MeV/c^2 of the nominal ϕ mass, both kaon candidates were required to be identified as "very loose" kaons, otherwise to be identified as "loose" kaons.

For the $D_s^- \to K^{*0}K^-$ decay mode, the invariant mass of the K^{*0} candidates was required to be within ± 60 MeV/c^2 of the nominal K^{*0} mass value and the K^{*0} momentum was required to exceed 5 GeV/c. The momentum of the K^- candidate from D_s^- was required to exceed 3 GeV/c. To suppress the physical background from the $D^- \to K^+\pi^-\pi^-$ kinematic reflection, the K^- candidate was required to be identified as a "standard" kaon. For $K^{*0} \to K^+\pi^-$ decays, "loose" identified K^+ were also accepted. In order to suppress the combinatorial background, the K^- candidate was required to be identified as "tight" kaon, if the invariant mass of the K^{*0} candidates was out of ± 20 MeV/c^2 of the nominal K^{*0} mass value, and the value of $|\cos\psi|$ was required to be larger than 0.8.

The selection of a hadron accompanying the D_s candidate is based on an impact parameter technique. A sample of tracks coming predominantly from B hadron decays was preselected by using their impact parameters and the corresponding errors, both with respect to the primary vertex (Im_p, σ_p) and to the secondary D_s decay vertex (Im_s, σ_s). The hadron was then searched for amongst the preselected particles in the event, by requiring that its charge was opposite to the D_s charge and that it had the largest momentum. The efficiency of the hadron selection was about 80% and, among the selected hadrons, (84±4)% came from a B vertex. Details on the track preselection as well as on the hadron selection are given in [27].

The B decay vertex was reconstructed by fitting the selected hadron and the D_s candidate to a common vertex. The χ^2–probability of the fitted B_s^0 vertex has been required to be larger than 10^{-3}. In order to increase the resolution on the measured decay length, only reconstructed events with a decay length error smaller than 0.07 cm were kept.

If the previous procedure failed, a new attempt was made, using an inclusive algorithm which allowed several hadrons to be attached to the D_s candidate. This algorithm is based on the difference in the rapidity distributions for particles coming from fragmentation and from B decays. The fragmentation particles, on average, have lower rapidity [29] than B decay products. The charged particles were ordered in increasing values of the rapidity and were attached in turn to the secondary D_s vertex. Up to three particles were accepted with their total charge equal to ±1 or 0. The rapidity was calculated as $0.5 \log((E + P_L)/(E - P_L))$, where E is the energy of the particle (assumed to be a pion) and P_L its longitudinal momentum with respect to the thrust axis of the event. Only particles with a momentum greater than 1 GeV/c were accepted. In addition, for the tracks satisfying the condition $Im_p/\sigma_p < 3$, it was required that $Im_s/\sigma_s < Im_p/\sigma_p$. Events with a decay length error smaller than 0.07 cm and a χ^2–probability of the fitted B_s^0 vertex larger than 10^{-3} were kept.

The selected sample, specified as $D_s^{\pm}h^{\mp}$ in the following, contained about 30% of such "multi-hadron" events. Among them, about 20% have one, 50% two and 30% three selected hadrons. The multi-hadron and single-hadron events were treated in a similar way. Figure 7 shows the D_s signals after selection of the accompanying hadron(s). The mass distributions were fitted with two Gaussian functions of equal widths to account for the D_s^- and D^- signals and with an exponential function for the combinatorial background. All parameters were allowed to vary in the fit. Table 5 gives the number of observed events in the D_s signal, after background subtraction, and the fraction of combinatorial background. The D_s signal region corresponds to a mass interval of $\pm 2\sigma$ centred on the fitted D_s mass.

The reconstructed number of $D_s^- \to \phi\pi^-$ events using 1994-1995 data is about 1.5 larger than those obtained using 1992-1993 data. This factor reflects the difference in statistics between the two data sets. Such "statistical scaling" does not apply to the $D_s^- \to K^{*0}K^-$ decay mode, where the particle identification, which was better for the 1994-1995 data set (see Sect. 2), plays a more important role.

Four events are in common with the exclusively reconstructed B_s^0 sample: one event in the main peak and three in the satellite peak. These events were removed from the $D_s^{\pm}h^{\mp}$ sample for the oscillation analysis.

4.2 Sample composition

The $D_s^{\pm}h^{\mp}$ sample contained a large physical background due to D_s from non-strange B hadron decays and from $c\bar{c}$ fragmentation. Four sources of events, originating from B decays, were considered: two from B_s^0 and two from non-B_s^0 mesons, namely, B decaying to one or two charmed mesons comprising at least one D_s. The relative fractions of these sources were calculated using five input parameters:

- $Br(b \to D_s^{\pm}X)$ at LEP [30];
- $Br(b \to D_s^{\pm}X)$ at $\Upsilon(4S)$ [31];

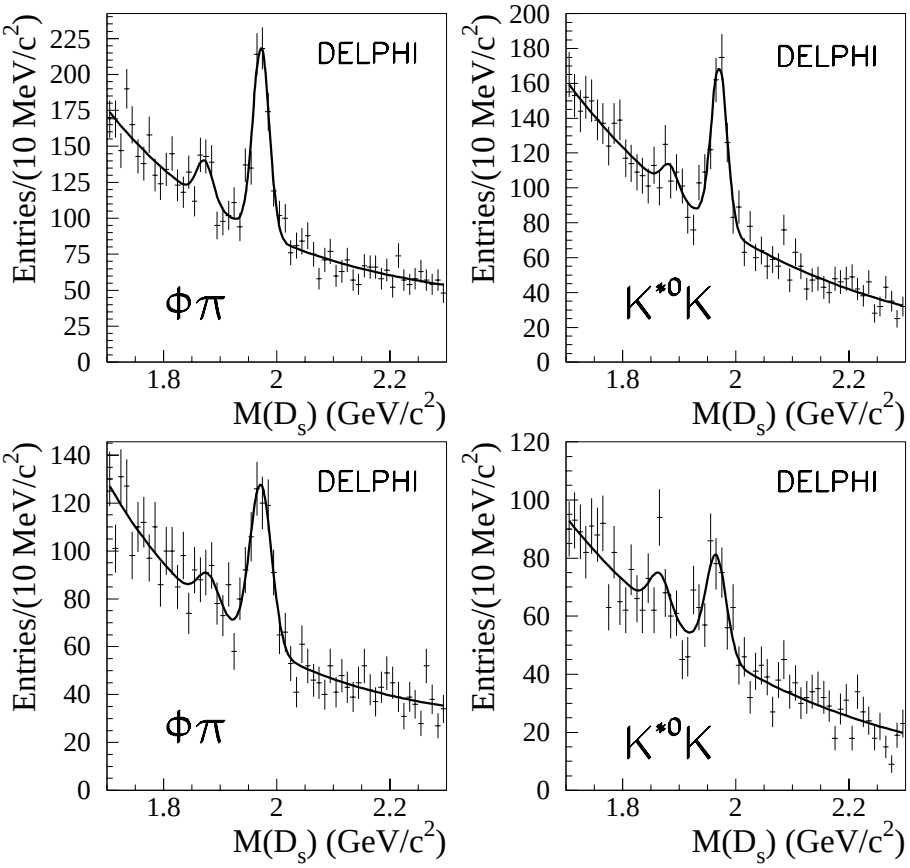

Fig. 7. Invariant mass distributions for D_s candidates selected in $\phi\pi^-$ and $K^{*0}K^-$ decay channels. The upper and lower plots refer to data samples registered in 1994-1995 and 1992-1993, respectively. The selected D_s candidates are accompanied by a hadron of opposite charge (or by several hadrons), measured in the same event hemisphere. The curves show the fits described in the text

– $Br(b \to \overline{B_s^0})$ at LEP [25];
– the probability in the non-strange B meson, that a D_s^- is produced at the lower vertex: $Br(B_{u,d} \to D_s^- X)$ [32];
– the probability to have two charmed hadrons in a b-decay: $Br(b \to D\overline{D}X)$ [33].

The last two probabilities were assumed to be the same for all B species. To estimate the first two branching fractions, the averaged production rate of D_s from all B species,

$Br(b \to D_s^{\pm} X) \times Br(D_s^{\pm} \to \phi\pi^{\pm})$, measured by the ALEPH, DELPHI and OPAL collaborations [30], and the equivalent quantity $Br(B_{u,d} \to D_s^{\pm} X) \times Br(D_s^{\pm} \to \phi\pi^{\pm})$, measured at the $\Upsilon(4S)$ by the CLEO and ARGUS collaborations [31], were used. The following fractions for the different B decays contributing to the $D_s^{\pm}h^{\mp}$ signal were evaluated:

– Fraction of B_s^0 decaying to a D_s and no other charmed meson: $F_{B_s,1D}=(39 \pm 7)\%$.
– Fraction of B_s^0 decaying to a D_s and another charmed meson: $F_{B_s,2D}=(11 \pm 3)\%$.
– Fraction of B mesons (non-B_s^0) decaying to a D_s and no other charmed meson: $F_{B,1D}=(9 \pm 5)\%$.
– Fraction of B mesons (non-B_s^0) decaying to a D_s and another charmed meson: $F_{B,2D}=(41 \pm 7)\%$.

The contribution F_{cc} from direct charm was estimated from the measurement of D_s production in charm events at LEP [30], taking into account the Z partial widths into b and c quark pairs: $F_{cc}=(27 \pm 5)\%$.

Finally, the relative proportion of the combinatorial background f_{bkg} was taken directly from the fit of the real data mass distributions (see Table 5).

4.3 Discriminant variables to increase the B_s^0 purity

To increase the effective purity in B_s^0 of the selected sample, five variables were used which allow the separation of the signal and background components. These variables are: the D_s mass, the D_s momentum, the value of $|\cos\psi|$, the χ^2–probability of the fitted D_s decay vertex and the value of the b-tagging variable measured in the hemisphere opposite to that of the D_s meson.

The relative components in the selected sample, defined in the previous section, were calculated on an event-by-event basis:

$$f^{eff}_{B_s,1D} = F_{B_s,1D}(1 - f_{cc} - f_{bkg})\mathcal{F}_b(b - tag) \times \prod_{i=1,4} \mathcal{F}_{bc}(v_i)/tot$$

$$f^{eff}_{B_s,2D} = F_{B_s,2D}(1 - f_{cc} - f_{bkg})\mathcal{F}_b(b - tag) \times \prod_{i=1,4} \mathcal{F}_{bc}(v_i)/tot$$

$$f^{eff}_{B,1D} = F_{B,1D}(1 - f_{cc} - f_{bkg})\mathcal{F}_b(b - tag) \times \prod_{i=1,4} \mathcal{F}_{bc}(v_i)/tot$$

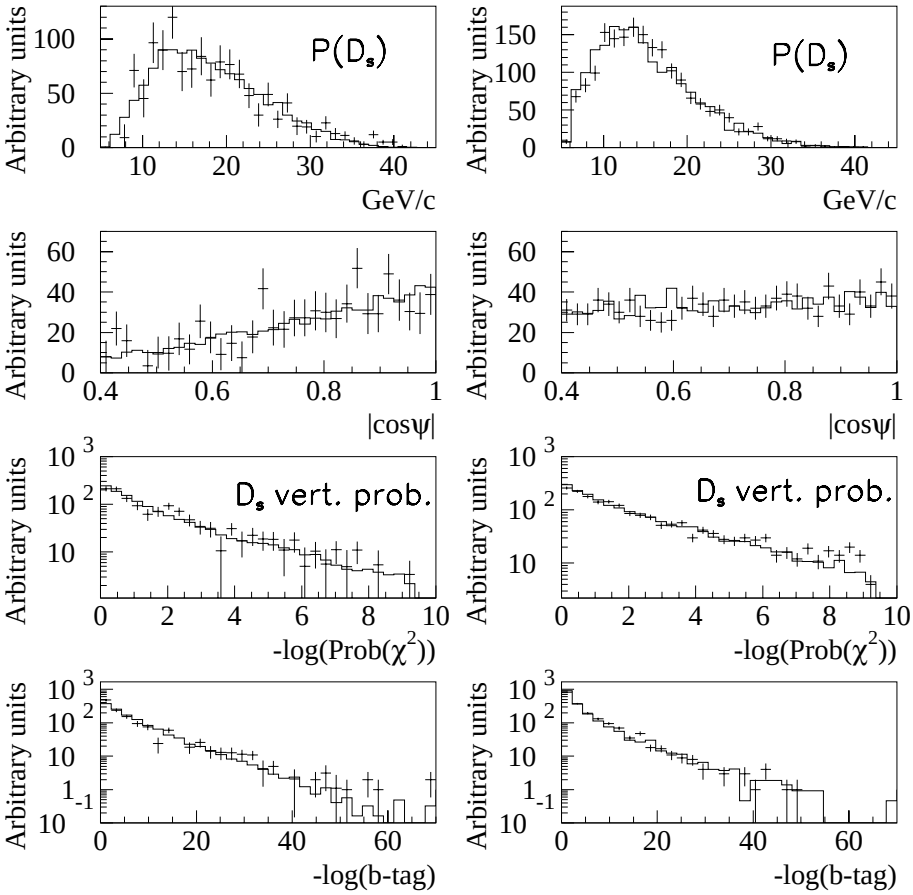

Fig. 8. Distributions of the variables used to increase the B_s purity. The distributions on the left are for events selected in the signal region after having subtracted the corresponding distributions of background events, which have been obtained using events situated in the side-bands of the D_s signal. The corresponding distributions for background events are shown on the right. The points with error bars correspond to the data and the histograms are simulated events. For the $|\cos\psi|$ distribution, only the $\phi\pi^+$ decay mode is shown because the cut on this variable was set at 0.6 for $K^{*0}K^-$ and at 0.4 for $\phi\pi^+$ channel. In addition, the D_s mass was used as the fifth discriminating variable: the signal has a Gaussian and the background has an exponential distribution

$$f^{eff}_{\mathrm{B,2D}} = F_{\mathrm{B,2D}}(1 - f_{cc} - f_{bkg})\mathcal{F}_{\mathrm{b}}(\mathrm{b}-tag) \times \prod_{i=1,4} \mathcal{F}_{\mathrm{bc}}(v_i)/tot$$

$$f^{eff}_{\mathrm{cc}} = f_{cc}\mathcal{F}_{\mathrm{c}}(\mathrm{b}-tag) \prod_{i=1,4} \mathcal{F}_{\mathrm{bc}}(v_i)/tot$$

$$f^{eff}_{bkg} = f_{bkg} \prod_{i=1,5} \mathcal{F}_{bkg}(v_i)/tot$$

where v_i indicates the i-th discriminant variable, $\mathcal{F}_{\mathrm{bc}}$, $\mathcal{F}_{\mathrm{b}}$, $\mathcal{F}_{\mathrm{c}}$ and $\mathcal{F}_{bkg}$ are the probability density functions for the b and c together, b, c and the combinatorial background events, respectively. The relative charm contribution is $f_{cc} = F_{cc}(1 - f_{bkg})$. In these expressions, the total normalisation factor is:

$$tot = f^{eff}_{\mathrm{B_s,1D}} + f^{eff}_{\mathrm{B_s,2D}} + f^{eff}_{\mathrm{B,1D}} + f^{eff}_{\mathrm{B,2D}} + f^{eff}_{\mathrm{cc}} + f^{eff}_{bkg}.$$

All discriminant variables, except for the b-tagging, were used to separate b and c events together from the combinatorial background (bkg). The b-tagging variable was used to distinguish separately the b from c and from combinatorial background events. The distributions of discriminant variables are shown in Fig. 8 for events selected in the signal region, after having subtracted the corresponding distributions of background events obtained using events within the side-bands of the D_s signal. The corresponding distributions for background events are also shown in Fig. 8. For the b-tagging variable, comparison with simulation is shown for the sum of the b and c events. The agreement between real data and simulated distributions is satisfactory.

The use of this procedure is equivalent to increase the B_s^0 purity by 20%.

4.4 Measurement of the B_s^0 lifetime

4.4.1 Proper time resolution

For each event, the B_s^0 proper decay time was obtained from the measured decay length ($L_{B_s^0}$) and the estimate of the B_s^0 momentum ($p_{B_s^0}$). The technique used is described in [27]. The predicted decay time distributions were obtained by convoluting the theoretical distributions with resolution functions evaluated from simulated events. Different parameterisations were used for the two Vertex Detector configurations installed in 1992-1993 and 1994-1995. The proper time resolution was obtained from the (t-t_i) distribution of the difference between the generated (t) and the reconstructed (t_i) proper times. The following distributions were considered:

– $\mathcal{R}_{\mathrm{B,1D}}(t - t_i)$ is the resolution function for B decays with only one charmed meson (D_s) in the final state. It is parameterised as the sum of three Gaussian functions. The width of the second Gaussian is taken to

Table 6. Fitted values of the parameters used in the resolution functions $\mathcal{R}_{\rm B,1D}(t-t_i)$ and $\mathcal{R}_{\rm B,2D}(t-t_i)$

	$D_s^{\pm}h^{\mp}$ sample							
Resol. function (years)	σ_{L1}(ps)	σ_{p1}/p	σ_{L3}(ps)	σ_{p3}/p	f_2	s_1	s_2	s_3 (ps^{-1})
$\mathcal{R}^{\rm B}_{\rm 1D}(t-t_i)$ (1992-1993)	0.149	0.140	0.144	0.386	0.15	3.5	-1.54	0.14
$\mathcal{R}^{\rm B}_{\rm 1D}(t-t_i)$ (1994-1995)	0.145	0.104	0.169	0.256	0.10	2.5	-1.87	0.17
$\mathcal{R}^{\rm B}_{\rm 2D}(t-t_i)$ (1992-1993)	0.236	0.095	0.144	0.386	0.30	3.5	-1.21	0.14
$\mathcal{R}^{\rm B}_{\rm 2D}(t-t_i)$ (1994-1995)	0.214	0.094	0.169	0.256	0.25	3.5	-1.30	0.17

be proportional to the width of the first one. The third Gaussian describes the component with a selected hadron coming from the primary vertex; the fraction (f_3) of these events decreases exponentially as a function of the proper time:

$$\mathcal{R}_{\rm B,1D}(t-t_i) = (1-f_2-f_3)G_1(t-t_i,\sigma_1) + f_2G_2(t-t_i,\sigma_2) + f_3G_3(t-t_i,\sigma_3) \quad (18)$$

where $G_1(t-t_i,\sigma_1)$, $G_2(t-t_i,\sigma_2)$ and $G_3(t-t_i,\sigma_3)$ are Gaussian functions with $\sigma_1 = \sqrt{\sigma_{L1}^2 + (\sigma_{p1}/p)^2 \times t^2}$, $\sigma_2 = s_1\sigma_1$, $\sigma_3 = \sqrt{\sigma_{L3}^2 + (\sigma_{p3}/p)^2 \times t^2}$; f_2 and f_3 are the fractions of the second and third Gaussian functions, respectively; f_3 is defined as $f_3 = \exp(s_2 - s_3 t)$. The values for the decay length resolutions, σ_{Lj}, the momentum resolutions, σ_{pj}/p, the relative fractions, f_j, and the coefficients s_j, are given in Table 6.

– $\mathcal{R}_{\rm B,2D}(t-t_i)$ is the resolution function for B decays with two D mesons in the final state. In this case, the selected hadron often does not originate directly from the B vertex, but from the second D vertex, hence resulting in a worse resolution. This resolution function is parameterised in a similar way as $\mathcal{R}_{\rm B,1D}(t-t_i)$ and the values of the corresponding parameters are shown in Table 6.

4.4.2 Likelihood fit

The B_s^0 mean lifetime and the time distribution of the combinatorial background were fitted simultaneously, using selected events lying within a mass interval of $\pm 2\sigma$ centred on the measured D_s mass (2953 events) and events lying in the D_s mass side-band (3373 events) between 2.1 and 2.3 GeV/c^2. The probability density function for the measured proper time, t_i, can be written as:

$$P(t_i) = f^{eff}_{\rm B_s,1D}P_{\rm B_s,1D}(t_i) + f^{eff}_{\rm B_s,2D}P_{\rm B_s,2D}(t_i) + f^{eff}_{\rm B,1D}P_{\rm B,1D}(t_i) + f^{eff}_{\rm B,2D}P_{\rm B,2D}(t_i) + f^{eff}_{\rm cc}P_{cc}(t_i) + f^{eff}_{bkg}P_{bkg}(t_i). \quad (19)$$

The different probability densities are expressed as convolutions of the physical probability densities with the appropriate resolution functions:

– For the signal:

$$P_{\rm B_s,1D}(t_i) = \frac{1}{\tau_{\rm B_s^0}}\exp(-t/\tau_{\rm B_s^0}) \otimes \mathcal{R}_{\rm B,1D}(t-t_i)$$

$$P_{\rm B_s,2D}(t_i) = \frac{1}{\tau_{\rm B_s^0}}\exp(-t/\tau_{\rm B_s^0}) \otimes \mathcal{R}_{\rm B,2D}(t-t_i),$$

where t is the true proper time.

– For the physical background coming from all B meson decays:

$$P_{\rm B,1D}(t_i) = \sum_{q\neq s}\frac{1}{\tau_{\rm B_q}}f_{\rm B_q,1D}\ \exp(-t/\tau_{\rm B_q}) \otimes \mathcal{R}_{\rm B,1D}(t-t_i)$$

$$P_{\rm B,2D}(t_i) = \sum_{q\neq s}\frac{1}{\tau_{\rm B_q}}f_{\rm B_q,2D}\ \exp(-t/\tau_{\rm B_q}) \otimes \mathcal{R}_{\rm B,2D}(t-t_i).$$

where q runs over the various b-hadron species contributing to this background and $f_{\rm B_q,1D}$, $f_{\rm B_q,2D}$ are their corresponding fractions.

– For the combinatorial background, the following function was used:

$$P_{bkg}(t_i) = f^-\exp(t/\tau^-) \otimes G(t-t_i,\sigma_-) + f^+\exp(-t/\tau^+) \otimes G(t-t_i,\sigma_+) + (1-f^- - f^+)G(t-t_i,\sigma_0)$$

Three distributions were considered: an exponential for poorly measured events having negative t (with lifetime τ^-), an exponential for the flying background (with lifetime τ^+) and a central Gaussian for the non-flying one. The seven parameters (f^-, f^+, τ^+, τ^-, σ_-, σ_+, σ_0) were allowed to vary in the fit.

– For "charm" candidates, the function $P_{\rm cc}(t_i)$ has the same form as $P_{bkg}(t_i)$ and has been parameterised using simulated events. In this case all the parameters were fixed in the fit.

The B_s^0 lifetime fit was performed in the proper time interval between -4 ps and 12 ps and the result of the fit, shown in Fig. 9, is:

$$\tau_{\rm B_s^0} = \ 1.53\ ^{+0.16}_{-0.15}\ (stat.)\ {\rm ps}.$$

4.4.3 Systematic uncertainties on the B_s^0 lifetime

The contributions to systematic uncertainties on the B_s^0 lifetime measurement are summarised in Table 7.

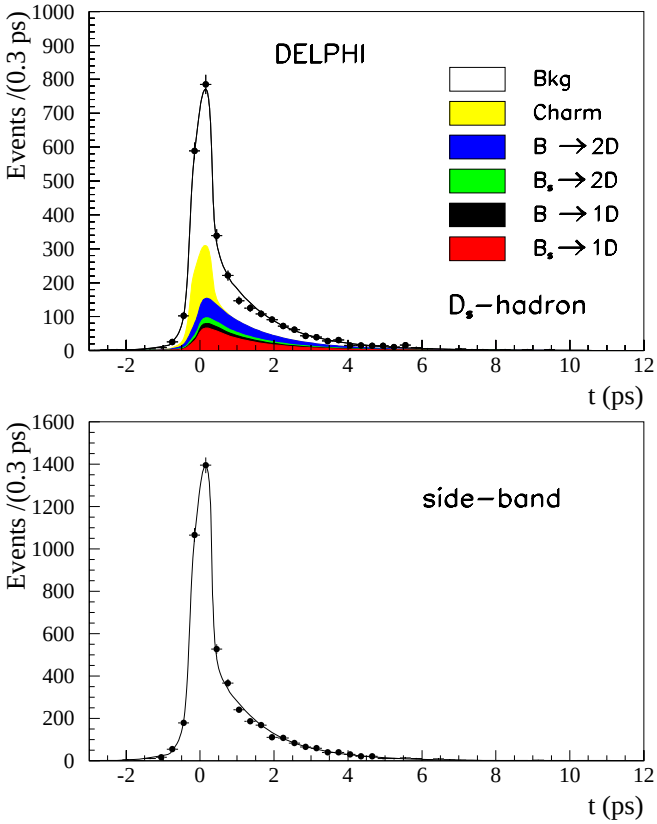

Fig. 9. $D_s^{\pm}h^{\mp}$ analysis. Upper plot: Proper time distribution for events in the signal mass region. The points show the data and the shaded regions correspond to the different contributions to the selected events. The curve shows the result of the fit described in the text. Lower plot: the same as the upper plot but for events situated in the D_s mass side-band

Table 7. Sources of systematic uncertainties on the B_s^0 lifetime

Source of systematic uncertainty	$\tau_{B_s^0}$ variation (ps)
Sample composition	$^{+0.013}_{-0.016}$
f_{bkg}	$^{+0.046}_{-0.050}$
B_s purity	$^{+0.005}_{-0.015}$
t resolution	± 0.019
$\tau_{B^+}(1.65 \pm 0.03$ ps) [7]	± 0.016
$\tau_{B_d^0}(1.56 \pm 0.03$ ps) [7]	± 0.014
Analysis bias correction	± 0.040
Total	± 0.07

The systematic error due to the uncertainties in the relative fractions of the different D_s sources corresponds to a $\pm 1\sigma$ variation of the fractions f used in the likelihood fit, excluding f_{bkg} which is studied separately.

The estimate of systematics related to the evaluation of the B_s^0 purity, on an event-by-event basis, was obtained in the following way. The distributions of the different quantities contributing to the discriminant variable (Fig. 8) for signal and background events were re-weighted with a linear function in order to maximise the agreement between data and the simulation. The B_s lifetime distribution was refitted with new probability distributions and the difference between the corresponding values of the fitted lifetime taken as a systematic error.

Uncertainties on the determination of the resolution of the proper time receive two contributions: one from errors on the decay distance evaluation and the other from errors on the measurement of the B_s^0 momentum. The systematic error coming from uncertainties on the time resolution was evaluated by varying the widths σ_L and σ_p of the resolution function by $\pm 10\%$ [10,27,28]. Finally, simulated B_s^0 events, generated with a lifetime of 1.6 ps and satisfying the same selection criteria as the real data, have a fitted lifetime of 1.64 ± 0.04 ps. The B_s^0 lifetime value obtained in the Sect. 4.4.2 was not corrected but the statistical error of this comparison (± 0.04 ps) was included in the systematic error. The measured B_s^0 lifetime was found to be:

$$\tau_{B_s^0} = 1.53^{+0.16}_{-0.15}(stat.) \pm 0.07(syst.) \text{ p}s.$$

A similar analysis by the ALEPH collaboration [12] gave a consistent result: $\tau_{B_s^0} = 1.47 \pm 0.14(stat.) \pm 0.08(syst.)$ ps.

4.5 Lifetime difference between B_s^0 mass eigenstates

The B_s^0 (or $\overline{B_s^0}$) mesons are superpositions of the two mass eigenstates:

$$|B_s^0\rangle = \frac{1}{\sqrt{2}}\left(|B_H^0\rangle + |B_L^0\rangle\right) \;;\; |\overline{B}_s^0\rangle = \frac{1}{\sqrt{2}}\left(|B_H^0\rangle - |B_L^0\rangle\right).$$

Neglecting CP violation, the time probability density is then given by:

$$\mathcal{P}(t) = (1 - x_{cp})\frac{\Gamma_H \Gamma_L}{\Gamma_H + \Gamma_L}\left(e^{-\Gamma_H t} + e^{-\Gamma_L t}\right) + x_{cp}\Gamma_L e^{-\Gamma_L t} \quad (20)$$

where $\Gamma_L = \Gamma_{B_s^0} + \Delta\Gamma_{B_s^0}/2$, $\Gamma_H = \Gamma_{B_s^0} - \Delta\Gamma_{B_s^0}/2$.

The first term of (20) refers to final states of identified beauty flavor, as in the $D_s\ell$ case [10], it does include D_s+light mesons final states. The second term corresponds to $D_s^{(*)+}D_s^{(*)-}$ final states, which are dominantly (98%) CP even eigenstates [34]. The value of x_{cp} was taken as the ratio of $F_{B_s,2D}$ to $(F_{B_s,1D}+F_{B_s,2D})$: $x_{cp} = 0.22 \pm 0.07$ (see Sect. 4.2).

Two variables are then considered: $\tau_{B_s^0}$ $(1/\Gamma_{B_s^0})$ and $\Delta\Gamma_{B_s^0}/\Gamma_{B_s^0}$. As the statistics in the sample is not sufficient to fit simultaneously $\tau_{B_s^0}$ and $\Delta\Gamma_{B_s^0}/\Gamma_{B_s^0}$, the method used to evaluate $\Delta\Gamma_{B_s^0}/\Gamma_{B_s^0}$ consists in calculating the log-likelihood for the time distribution measured with the $D_s^{\pm}h^{\mp}$ sample and deriving the probability density function for $\Delta\Gamma_{B_s^0}/\Gamma_{B_s^0}$ by constraining $\tau_{B_s^0}$ to be equal to the B_d^0 lifetime ($\tau_{B_d^0} = 1.56 \pm 0.03$ ps [7] and $\tau_{B_s^0}/\tau_{B_d^0} = 1 \pm \mathcal{O}(0.01)$ is predicted in [14]).

The log-likelihood function described in Sect. 4.4.2 was modified by replacing the probability density for B_s^0 by

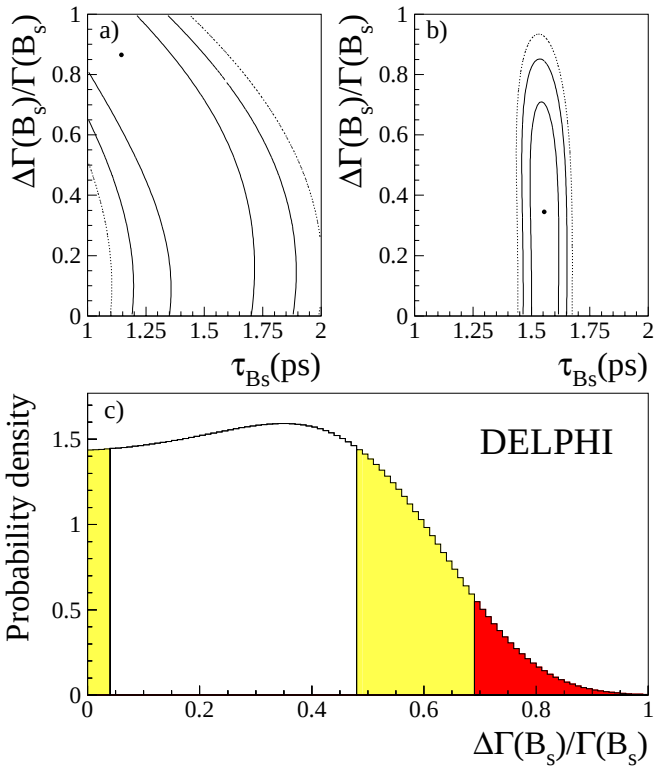

Fig. 10a–c. $D_s^{\pm}h^{\mp}$ analysis: 68%, 95%, 99% C.L. contours of the negative log-likelihood in the plane $\Delta\Gamma_{B_s^0}/\Gamma_{B_s^0} - \tau_{B_s^0}$ **a** without and **b** with $\tau_{B_s^0} = \tau_{B_d^0}$ constraint. The point indicates the minimum. **c** Probability density distribution for $\Delta\Gamma_{B_s}/\Gamma_{B_s}$; the two lightly shaded regions at the 68% C.L. and dark one at the 95% C.L. are also shown

(20) convoluted with the appropriate resolution functions. It was minimized in the $(\tau_{B_s^0}, \Delta\Gamma_{B_s^0}/\Gamma_{B_s^0})$ plane and the likelihood difference with respect to its minimum $\Delta\mathcal{L}$ (Fig. 10a) was computed:

$$\Delta\mathcal{L} = -\log\mathcal{L}_{tot}(\tau_{B_s^0}, \Delta\Gamma_{B_s^0}/\Gamma_{B_s^0}) + \log\mathcal{L}_{tot}\left((\tau_{B_s^0})^{min}, (\Delta\Gamma_{B_s^0}/\Gamma_{B_s^0})^{min}\right) .$$

The probability density function for the variables $\tau_{B_s^0}$ and $\Delta\Gamma_{B_s^0}/\Gamma_{B_s^0}$ is proportional to:

$$\mathcal{P}(\tau_{B_s^0}, \Delta\Gamma_{B_s^0}/\Gamma_{B_s^0}) \propto e^{-\Delta\mathcal{L}}.$$

The $\Delta\Gamma_{B_s^0}/\Gamma_{B_s^0}$ probability distribution was then obtained by convoluting $\mathcal{P}(\tau_{B_s^0}, \Delta\Gamma_{B_s^0}/\Gamma_{B_s^0})$ with the probability density function $f_{(\tau_{B_s^0}=\tau_{B_d^0})}(\tau_{B_s^0})$, expressing the constraint $\tau_{B_s^0} = \tau_{B_d^0}$, and normalising the result to unity:

$$\mathcal{P}(\Delta\Gamma_{B_s^0}/\Gamma_{B_s^0}) = \left\{\int \mathcal{P}(\tau_{B_s^0}, \Delta\Gamma_{B_s^0}/\Gamma_{B_s^0}) f_{(\tau_{B_s^0}=\tau_{B_d^0})}(\tau_{B_s^0}) d\tau_{B_s^0}\right\} \Big/ \left\{\int \mathcal{P}(\tau_{B_s^0}, \Delta\Gamma_{B_s^0}/\Gamma_{B_s^0}) f_{(\tau_{B_s^0}=\tau_{B_d^0})} \times(\tau_{B_s^0}) d\tau_{B_s^0} d\Delta\Gamma_{B_s^0}/\Gamma_{B_s^0}\right\}$$

where

$$f_{\left(\tau_{B_s^0}=\tau_{B_d^0}\right)}\left(\tau_{B_s^0}\right) = 1/\left(\sqrt{2\pi}\sigma_{\tau_{B_d^0}}\right) \times \exp\left(-(\tau_{B_s^0} - \tau_{B_d^0})^2/2\sigma^2_{\tau_{B_d^0}}\right).$$

The upper limit on $\Delta\Gamma_{B_s^0}/\Gamma_{B_s^0}$, calculated from $\mathcal{P}(\Delta\Gamma_{B_s^0}/\Gamma_{B_s^0})$, is:

$$\Delta\Gamma_{B_s^0}/\Gamma_{B_s^0} < 0.67 \text{ at the } 95\% \text{ C.L.}$$

This limit takes into account both statistical uncertainties and the systematic coming from the uncertainty[5] on the B_d^0 lifetime.

The systematic uncertainty originating from other sources was evaluated by convoluting the probability function $\mathcal{P}(\tau_{B_s^0}, \Delta\Gamma_{B_s^0}/\Gamma_{B_s^0})$ with the probability function of the corresponding parameters:

$$\mathcal{P}(\Delta\Gamma_{B_s^0}/\Gamma_{B_s^0}) = \left\{\int \mathcal{P}\left(\tau_{B_s^0}, \Delta\Gamma_{B_s^0}/\Gamma_{B_s^0}, x^1_{sys}, ..., x^n_{sys}\right) f_{\left(\tau_{B_s^0}=\tau_{B_d^0}\right)} \times\left(\tau_{B_s^0}\right) f\left(x^1_{sys}\right) ... f\left(x^n_{sys}\right) d\tau_{B_s^0} dx^1_{sys} ... dx^n_{sys}\right\} \Big/ \left\{\int \mathcal{P}\left(\tau_{B_s^0}, \Delta\Gamma_{B_s^0}/\Gamma_{B_s^0}, x^1_{sys}, ..., x^n_{sys}\right) f_{\left(\tau_{B_s^0}=\tau_{B_d^0}\right)} \times\left(\tau_{B_s^0}\right) f\left(x^1_{sys}\right) ... f\left(x^n_{sys}\right) d\tau_{B_s^0} dx^1_{sys} ... dx^n_{sys} \times d\Delta\Gamma_{B_s^0}/\Gamma_{B_s^0}\right\}$$

where x^i_{sys} are the n parameters considered in the systematic uncertainty and $f(x^i_{sys})$ are the corresponding probability densities.

Only three systematics were considered here: the relative fraction of combinatorial background f_{bkg}, the B_s^0 purity of the selected sample and the x_{cp} fraction. Other systematic uncertainties are expected to be small as they are in the lifetime measurement.

The $\Delta\Gamma_{B_s^0}/\Gamma_{B_s^0}$ probability distribution, obtained with the inclusion of the systematics, is shown in Fig. 10c, the most probable value for $\Delta\Gamma_{B_s^0}/\Gamma_{B_s^0}$ is 0.35 and the upper limit at the 95% confidence level is:

$$\Delta\Gamma_{B_s^0}/\Gamma_{B_s^0} < 0.69 \text{ at the } 95\% \text{ C.L.}$$

It should be noted that the world average of the B_s^0 lifetime cannot be used as a constraint in such an analysis, since it

[5] The uncertainty due to the theoretical prediction of the equality of the $\tau_{B_s^0}$ and $\tau_{B_d^0}$ lifetimes is negligible with respect to the present error on $\tau_{B_d^0}$

depends on $\Delta\Gamma_{B_s^0}$ and on $\Gamma_{B_s^0}$. Moreover, this dependence is also different for different decay channels. In the $D_s^{\pm}h^{\mp}$ case the expression of the average B_s^0 lifetime is given by:

$$\tau_{B_s^0}(D_s^{\pm}h^{\mp}) = (1-x_{cp})\frac{1+(\frac{1}{2}\Delta\Gamma_{B_s^0}/\Gamma_{B_s^0})^2}{\Gamma_{B_s^0}(1-(\frac{1}{2}\Delta\Gamma_{B_s^0}/\Gamma_{B_s^0})^2)}+x_{cp}/\Gamma_L\ . \quad (21)$$

4.6 Study of B_s^0-$\overline{B_s^0}$ oscillations

4.6.1 Tagging procedure

The tagging algorithm was explained in Sect. 3.5.1. An event is classified as a mixed or an unmixed candidate according to the relative signs of the D_s electric charge, Q_D, and of the tagging purity variable, x_{tag}.

Mixed candidates have $x_{tag}\cdot Q_D < 0$, and unmixed ones $x_{tag}\cdot Q_D > 0$. The probability, ϵ_b^{tag}, of tagging the b or the $\overline{b}$ quark correctly from the measurement of x_{tag} was evaluated using a dedicated simulated event sample. The average tagging purity of the x_{tag} variable, given by the simulation for true $B_s^0 \to D_s^- h^+ X$ decays, is $(71.4 \pm 0.4)\%$. The purity is lower than that obtained in the $D_s\ell$ sample [10] because not all B_s charged decay products are reconstructed in the present analysis. It was verified that the tagging purity is the same for different B hadron species and varies by less than about $\pm 2\%$ whether the B_s^0 has oscillated or not. This effect is taken into account in the systematics. The corresponding probability distribution for events in the combinatorial background was obtained using data candidates selected in the side-bands of the D_s signal: the probabilities of classifying these events as mixed or as unmixed candidates are called ϵ_{bkg}^{mix} and ϵ_{bkg}^{unmix}, respectively. For the charm events, the analogous probabilities are called ϵ_{cc}^{mix}, ϵ_{cc}^{unmix} and their values were taken from the simulation.

4.6.2 Fitting procedure

From the expected proper time distributions and the tagging probabilities, the probability functions for mixed and unmixed event candidates are

$$\begin{aligned} P^{mix}(t_i) = {} & f^{eff}_{B_s,1D}P^{mix}_{B_s,1D}(t_i) + f^{eff}_{B_s,2D}P^{mix}_{B_s,2D}(t_i) \\ & + f^{eff}_{B,1D}P^{mix}_{B,1D}(t_i) + f^{eff}_{B,2D}P^{mix}_{B,2D}(t_i) \\ & + f^{eff}_{cc}P^{mix}_{cc}(t_i) + f^{eff}_{bkg}P^{mix}_{bkg}(t_i), \end{aligned} \quad (22)$$

where t_i is the reconstructed proper time. The analytical expressions for the different probability densities are given in the following, with t being the true proper time:

– B_s^0 signal mixing probability:

$$\begin{aligned} P^{mix}_{B_s,1D}(t_i) = {} & \left\{\epsilon_b^{tag}\mathcal{P}^{mix}_{B_s,1D}(t) + (1-\epsilon_b^{tag})\mathcal{P}^{unmix}_{B_s,1D}(t)\right\} \\ & \otimes \mathcal{R}_{B,1D}(t-t_i) \end{aligned} \quad (23)$$

– Physical background mixing probabilities:

$$\begin{aligned} P^{mix}_{B_s,2D}(t_i) = {} & \left\{f_{B_s,2D}\epsilon_b^{tag}/\tau_{B_s^0}\exp(-t/\tau_{B_s^0})\right\} \\ & \otimes \mathcal{R}_{B,2D}(t-t_i) \end{aligned} \quad (24)$$

$$\begin{aligned} & P^{mix}_{B,1D}(t_i) \\ & = \Big\{f_{B_d,1D}(\epsilon_b^{tag}\mathcal{P}^{mix}_{B_d,1D}(t) + (1-\epsilon_b^{tag})\mathcal{P}^{unmix}_{B_d,1D}(t)) \\ & \quad + f_{B^+,1D}(1-\epsilon_b^{tag})/\tau_{B^+}\exp(-t/\tau_{B^+}) \\ & \quad + f_{\Lambda_b,1D}(1-\epsilon_b^{tag})/\tau_{\Lambda_b}\exp(-t/\tau_{\Lambda_b})\Big\} \\ & \quad \otimes \mathcal{R}_{B,1D}(t-t_i) \end{aligned} \quad (25)$$

$$\begin{aligned} & P^{mix}_{B,2D}(t_i) \\ & = \Big\{f_{B_d,2D}(\epsilon_b^{tag}\mathcal{P}^{unmix}_{B_d,2D}(t) + (1-\epsilon_b^{tag})\mathcal{P}^{mix}_{B_d,2D}(t)) \\ & \quad + f_{B^+,2D}(1-\epsilon_b^{tag})/\tau_{B^+}\exp(-t/\tau_{B^+}) \\ & \quad + f_{\Lambda_b,2D}(1-\epsilon_b^{tag})/\tau_{\Lambda_b}\exp(-t/\tau_{\Lambda_b})\Big\} \\ & \quad \times \otimes\, \mathcal{R}_{B,2D}(t-t_i) \end{aligned} \quad (26)$$

– Mixing probability for charm component:

$$P^{mix}_{cc}(t_i) = \epsilon^{mix}_{cc}\mathcal{P}_{cc}(t_i) \quad (27)$$

– Combinatorial background mixing probability:

$$P^{mix}_{bkg}(t_i) = \epsilon^{mix}_{bkg}\mathcal{P}_{bkg}(t_i) \quad (28)$$

The oscillation analysis was performed in the framework of the amplitude method [13] as described in Sect. 3.5.3. Considering only statistical uncertainties, the limit is:

$$\Delta m_{B_s^0} > 4.2\ \mathrm{ps}^{-1} \text{ at the } 95\% \text{ C.L.} \quad (29)$$

with a corresponding sensitivity equal to 3.1 ps^{-1}. At $\Delta m_{B_s^0} = 10\ \mathrm{ps}^{-1}$, the error on the amplitude is 2.3 (see Fig. 11).

4.6.3 Study of systematic uncertainties

Systematic uncertainties were evaluated by varying the parameters which were kept constant in the fit, according to their measured or expected errors.

– Systematics from the tagging probability:
a conservative variation of $\pm 3\%$ on the expected tagging probability for the signal and for the other three processes contributing to the $D_s^{\pm}h^{\mp}$ candidates was used. The same variation is assumed for the tagging purity for the charm and combinatorial background events. The central values of these purities were fixed to the simulated ones.

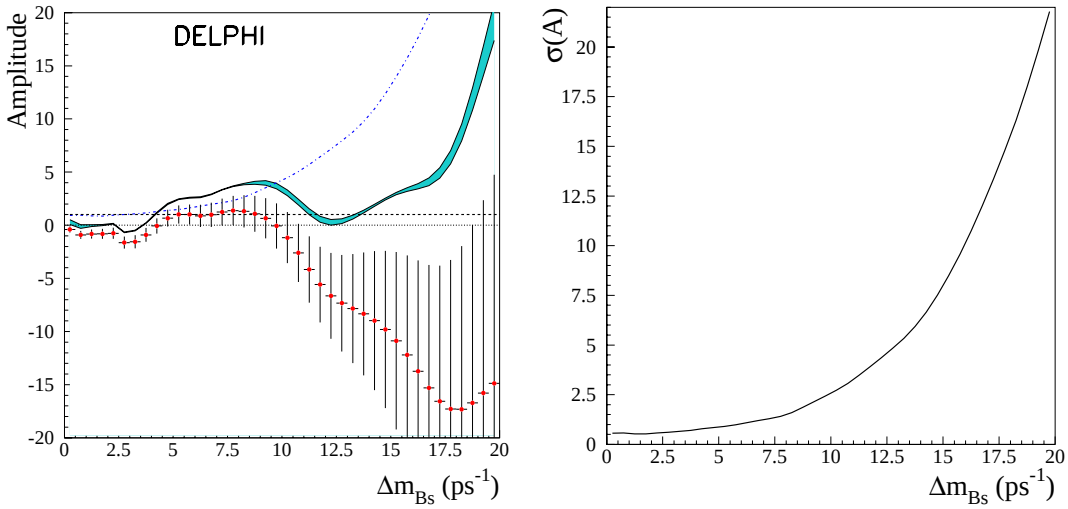

Fig. 11. $D_s^{\pm}h^{\mp}$ analysis. Left plot: variation of the oscillation amplitude A as a function of $\Delta m_{B_s^0}$. The lower continuous line corresponds to $A + 1.645\ \sigma(A)$ where $\sigma(A)$ includes statistical uncertainties only, while the shaded area shows the contribution from systematics. The dashed-dotted line corresponds to the sensitivity curve. The lines at A=0 and A=1 are also given. The points with error bars are real data. Right plot: variation of the error on the amplitude as a function of $\Delta m_{B_s^0}$, including systematic uncertainties

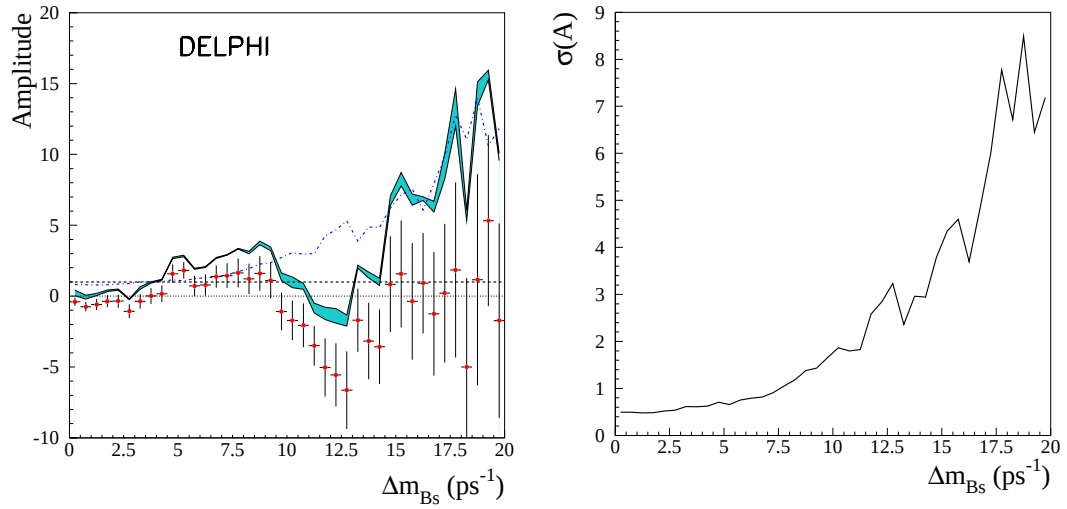

Fig. 12. Combination of the $D_s^{\pm}h^{\mp}$ and exclusive B_s^0 analyses. Left plot: variation of the oscillation amplitude A as a function of $\Delta m_{B_s^0}$. The lower continuous line corresponds to $A + 1.645\ \sigma(A)$ where $\sigma(A)$ includes statistical uncertainties only, while the shaded area shows the contribution from systematics. The dashed-dotted line corresponds to the sensitivity curve. The lines at A=0 and A=1 are also given.The points with error bars are real data. Right plot: variation of the error on the amplitude as a function of $\Delta m_{B_s^0}$ including systematic uncertainties. It should be noted that the $D_s^{\pm}h^{\mp}$ analysis dominates at low values of $\Delta m_{B_s^0}$ and the exclusive B_s^0 analysis dominates at large values of $\Delta m_{B_s^0}$

– Systematics from the B_s^0 purity:
the same procedure already applied to the lifetime measurement has been used.
– Systematics from the resolution on the B decay proper time:
the same procedure already applied to the lifetime measurement was used. In addition, the systematic error due to the variation of the proper time distribution of the combinatorial background was considered: the parameters used to define the background shape in the lifetime fit were varied according to their fitted errors.

The inclusion of systematic uncertainties lowers the sensitivity to 2.7 ps^{-1} and the 95% C.L limit becomes $\Delta m_{B_s^0} > 4.1\ ps^{-1}$.

The analogous analysis has been performed by the ALEPH collaboration [12], which set a limit at $\Delta m_{B_s^0} > 3.9\ ps^{-1}$ at the 95% C.L., with a better sensitivity of 4.1 ps^{-1}.

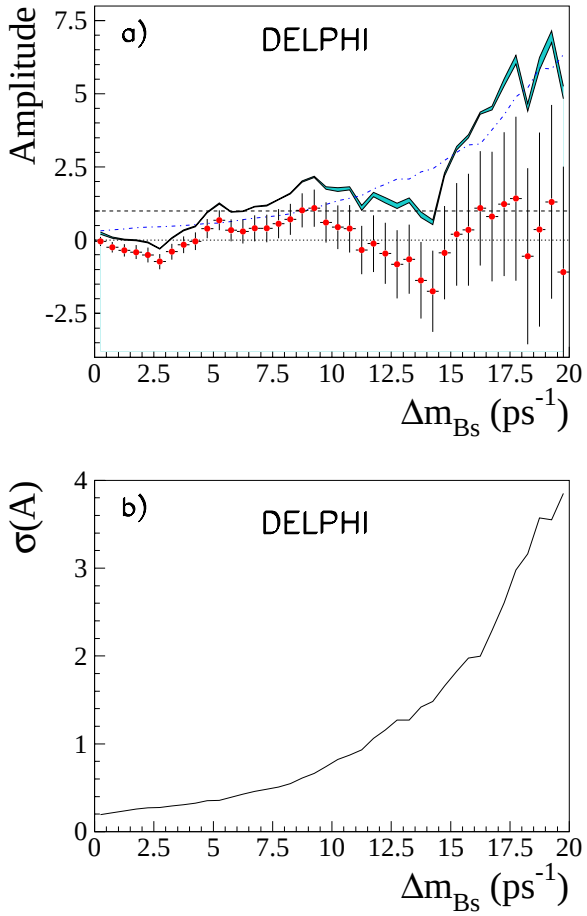

Fig. 13a,b. Combined DELPHI analysis: **a** variation of the oscillation amplitude A as a function of $\Delta m_{B_s^0}$. The lower continuous line corresponds to $A+1.645\,\sigma(A)$ where $\sigma(A)$ includes statistical uncertainties only, while the shaded area shows the contribution from systematics. The dashed-dotted line corresponds to the sensitivity curve. The lines at A=0 and A=1 are also given. The points with error bars are real data. **b** variation of the error on the amplitude as a function of $\Delta m_{B_s^0}$

5 Combined limit on $\Delta m_{B_s^0}$ using exclusive B_s^0 and $D_s^{\pm}h^{\mp}$ events

This paper presents two analyses on $\Delta m_{B_s^0}$ using exclusively reconstructed B_s^0 mesons and $D_s^{\pm}h^{\mp}$ events. Their results have been combined (Fig. 12), taking into account correlations between systematic uncertainties in the two amplitude measurements [7]. A limit at the 95% confidence level is obtained:

$$\Delta m_{B_s^0} > 4.0 \text{ ps}^{-1} \text{ at the 95\% C.L.} \qquad (30)$$

with a corresponding sensitivity equal to 3.2 ps^{-1} (with statistical errors only, the limit would be $\Delta m_{B_s^0} > 4.0\,\text{ps}^{-1}$ at the 95% C.L. with a sensitivity of 4.4 ps^{-1}). Figure 12 also shows the error on the amplitude for different values of $\Delta m_{B_s^0}$.

6 Combination of the DELPHI $\Delta m_{B_s^0}$, $\tau_{B_s^0}$ and $\Delta\Gamma_{B_s^0}/\Gamma_{B_s^0}$ analyses

DELPHI has performed three analyses on $\Delta m_{B_s^0}$ using $D_s^{\pm}\ell^{\mp}$ candidates [10], $D_s^{\pm}h^{\mp}$ events and exclusively reconstructed B_s^0 mesons. They were combined, taking into account correlations between the event samples and between systematic uncertainties in the different amplitude measurements (Fig. 13a). This gives the following limit for $\Delta m_{B_s^0}$:

$$\Delta m_{B_s^0} > 4.9 \text{ ps}^{-1} \text{ at the 95\% C.L.}$$
$$\text{with a sensitivity of } \Delta m_{B_s^0} = 8.7 \text{ ps}^{-1}$$

The exclusion probability for this limit is 88%. The variation, with $\Delta m_{B_s^0}$ of the error on the amplitude is given in Fig. 13b.

The results of two analyses on $\tau_{B_s^0}$ and $\Delta\Gamma_{B_s^0}/\Gamma_{B_s^0}$ using $D_s^{\pm}\ell^{\mp}$ and $D_s^{\pm}h^{\mp}$ events provide the following DELPHI results:

$$\tau_{B_s^0} = 1.46 \pm 0.11 \text{ ps}$$
$$\Delta\Gamma_{B_s^0}/\Gamma_{B_s^0} < 0.45 \text{ at the 95\% C.L.}$$

7 Conclusion

Using about 3.5 million hadronic Z decays registered by DELPHI between 1992 and 1995, two samples of events have been selected. The first one consists of 44 reconstructed B_s^0 events: 11 candidates (including 30% of background) are completely reconstructed and 33 candidates (including 55% of background) are partially reconstructed (π^0 and/or γ are not detected). This analysis used twelve different decay channels of the B_s^0 meson and is a first attempt to use such events for the oscillation studies. Due to the excellent proper time resolution, this sample gives some contribution in the high $\Delta m_{B_s^0}$ region.

The second sample contains 2953 $D_s^{\pm}h^{\mp}$ candidates (including 60% of background) with completely reconstructed D_s^- mesons in the $\phi\pi^-$ and $K^{*0}K^-$ decay channels. Using the $D_s^{\pm}h^{\mp}$ sample, three studies have been performed. The B_s^0 lifetime has been measured and a limit on the fractional width difference between the two physical B_s^0 states has been obtained:

$$\tau_{B_s^0} = 1.53^{+0.16}_{-0.15}(stat.) \pm 0.07(syst.) \text{ ps}$$

$$\Delta\Gamma_{B_s^0}/\Gamma_{B_s^0} < 0.69 \text{ at the 95\% C.L.}$$

This last result has been obtained under the hypothesis that $\tau_{B_s^0} = \tau_{B_d^0}$.

Combining the two studies on $B_s^0 - \overline{B_s^0}$ oscillations, a limit at the 95% C.L. on the mass difference between the physical B_s^0 states has been set:

$$\Delta m_{B_s^0} > 4.0 \text{ ps}^{-1} \text{ at the 95\% C.L.} \qquad (31)$$

with a corresponding sensitivity equal to 3.2 ps^{-1}.

Previous DELPHI results on B_s^0 lifetime obtained with the $D_s^{\pm}h^{\mp}$ sample [27] are superseded by the analysis presented in this paper.

Combination of the DELPHI $\Delta m_{B_s^0}$, $\tau_{B_s^0}$ and $\Delta\Gamma_{B_s^0}/\Gamma_{B_s^0}$ analyses gives:

$$\Delta m_{B_s^0} > 4.9\ ps^{-1} \text{ at the 95\% C.L.}$$
$$\text{with a sensitivity of } \Delta m_{B_s^0} = 8.7\ ps^{-1}$$

$$\tau_{B_s^0} = 1.46 \pm 0.11\ ps$$

$$\Delta\Gamma_{B_s^0}/\Gamma_{B_s^0} < 0.45 \text{ at the 95\% C.L.}$$

Acknowledgements. We are greatly indebted to our technical collaborators, to the members of the CERN-SL Division for the excellent performance of the LEP collider, and to the funding agencies for their support in building and operating the DELPHI detector. We acknowledge in particular the support of Austrian Federal Ministry of Science and Traffics, GZ 616.364/2-III/2a/98, FNRS–FWO, Belgium, FINEP, CNPq, CAPES, FUJB and FAPERJ, Brazil, Czech Ministry of Industry and Trade, GA CR 202/96/0450 and GA AVCR A1010521, Danish Natural Research Council, Commission of the European Communities (DG XII), Direction des Sciences de la Matière, CEA, France, Bundesministerium für Bildung, Wissenschaft, Forschung und Technologie, Germany, General Secretariat for Research and Technology, Greece, National Science Foundation (NWO) and Foundation for Research on Matter (FOM), The Netherlands, Norwegian Research Council, State Committee for Scientific Research, Poland, 2P03B06015, 2P03B1116 and SPUB/P03/178/98, JNICT–Junta Nacional de Investigação Científica e Tecnológica, Portugal, Vedecka grantova agentura MS SR, Slovakia, Nr. 95/5195/134, Ministry of Science and Technology of the Republic of Slovenia, CICYT, Spain, AEN96–1661 and AEN96-1681, The Swedish Natural Science Research Council, Particle Physics and Astronomy Research Council, UK, Department of Energy, USA, DE–FG02–94ER40817.

References

1. M. Beneke, G. Buchalla and I. Dunietz, Phys. Rev. **D54** (1996) 4419
2. L. Wolfenstein, Phys. Rev. Lett. **51** (1983) 1945
3. G. Altarelli and P.J. Franzini, Z. Phys. **C37** (1988) 271; P.J. Franzini, Phys Rep. **173** (1989) 1
4. A. J. Buras, Acta Phys. Polon. **B26** (1995) 755
5. A. Abada et al., Nucl. Phys. **B376** (1992) 172
6. P. Paganini, F. Parodi, P. Roudeau and A. Stocchi, Physica Scripta **58** (1998) 556; F. Parodi, P. Roudeau and A. Stocchi, Nuovo Cimento **112A** (1999) N.7
7. G. Blaylock. Dec 1999. Presented at 19th International Symposium on Lepton and Photon Interactions at High-Energies (LP 99), Stanford, California, 9-14 Aug 1999. e-Print Archive: hep-ex/9912038
8. D. Buskulic et al., ALEPH Coll., Eur. Phys. J. **C7** (1999) 553
9. G. Abbiendi et al., OPAL Coll., Eur. Phys. J. **C11** (1999) 587
10. P. Abreu et al., DELPHI Coll., "Measurement of the B_s^0 Lifetime and Study of $B_s^0 - \overline{B_s^0}$ Oscillations using $D_s - \ell$ Events", CERN-EP/2000-043, submitted to Eur. Phys. J. C
11. D. Buskulic et al., ALEPH Coll., Phys. Lett. **B377** (1996) 205
12. D. Buskulic et al., ALEPH Coll., Eur. Phys. J. **C4** (1998) 367
13. H.G. Moser and A. Roussarie, Nucl. Instr. Meth. **A384** (1997) 491
14. I. Bigi, Phys. Rep. **289** (1997) 1; M. Neubert, CERN-TH/98-2 (1998), invited talk at the International Europhysics Conference on High Energy Physics (HEP 97), Jerusalem, Israel (19-26 Aug 1997), ed. D. Lellouch, G. Mikenberg, E. Rabinovici (Springer, 1998)
15. M. Beneke et al., Phys. Lett. **B459** (1999) 631
16. P. Abreu et al., DELPHI Coll., Nucl. Instr. Meth. **A378** (1996) 57; E.G. Anassontzis et al., Nucl. Instr. Meth. **A323** (1992) 351
17. V. Chabaud et al., Nucl. Instr. Meth. **A368** (1996) 314
18. P. Abreu et al., DELPHI Coll., Nucl. Phys. **B418** (1994) 403
19. T. Sjöstrand, Comp. Phys. Commun. **82** (1994) 74
20. M. Battaglia and P.M. Kluit, Nucl. Instr. Meth. **A443** (1999) 252
21. G. Borisov and C. Mariotti, Nucl. Instr. Meth. **A372** (1996) 181
22. P. Abreu et al, DELPHI Coll., Z. Phys. **C73** (1996) 11
23. N. Isgur, et al, Phys. Rev. **D39** (1989) 799
24. A. Deandrea et al., Phys. Lett. **B318** (1993) 549
25. Review of Particle Physics, Eur. Phys. J. **C3** (1998) 1
26. M. Neubert and B. Stech, in A.J. Buras and M. Lindner (ed.): Heavy Flavours 2nd edition, p. 294-344. World Scientific, Singapore (1998)
27. P. Abreu et al., DELPHI Coll., Z. Phys. **C71** (1996) 11
28. W. Adam et al., DELPHI Coll., Phys. Lett. **B414** (1997) 382
29. P. Abreu et al., DELPHI Coll., Z. Phys. **C68** (1995) 353
30. G. Alexander et al., OPAL Coll., Z. Phys. **C72** (1996) 1; D. Buskulic et al., ALEPH Coll., Phys. Lett. **B388** (1996) 648; P. Abreu et al., DELPHI Coll., Eur. Phys. J. **C12** (2000) 225
31. H. Albrecht et al., ARGUS Coll., Z. Phys. **C54** (1992) 1; D.Gibaut et al., CLEO Coll., Phys. Rev. **D53** (1996) 4734
32. X.Fu et al.,CLEO Coll., Preprint CLEO-Conf 95-11
33. P.Abreu et al.,DELPHI Coll., Phys. Lett. **B426** (1998) 193
34. R. Aleksan, A. Le Yaouanc, L. Oliver, O. Pene and J.C. Raynal, Phys.Lett. **B316** (1993) 567